Quasi 2D and 1D van der Waals Materials – Properties and Device Applications

Alexander A. Balandin

Nano-Device Laboratory: NDL
Center for Phonon Optimized Engineered Materials: POEM
Department of Electrical and Computer Engineering
Materials Science and Engineering Program
University of California – Riverside

NSF 2DARE; NSF DMREF; DOE; SRC; DOE VBFF

MSE, UCLA – October 2021

| Nano-Device Laboratory >

Acknowledging Students Who Did the Work

Dr. G. Liu, Apple

Dr. R. Salgado, Intel

Dr. A. Geremew, Intel

Dr. E. Aytan, Intel

Dr. A. Mohammadzadeh, Indie Semiconductors

Dr. F. Kargar, UCR

Z. Barani, UCR

S. Baraghani, Lam Research

Highlights or Research Activities in NDL and POEM Center

Graphene thermal field and thermal management

- The MRS Medal

Quazi-1D van der Waals materials

- The Vannevar Buch Faculty Fellow
- NSF DMREF; DOD ONR

Nanoscale phonon engineering

- IEEE Pioneer of Nanotechnology Award
- DOE EFRC Ultra

Raman and Brillouin-Mandelstam spectroscopy

- The Brillouin Medal
- NSF MRI; NSF DMREF

Low-frequency noise spectroscopy

- DOE; DOE EFRC Ultra - ASU

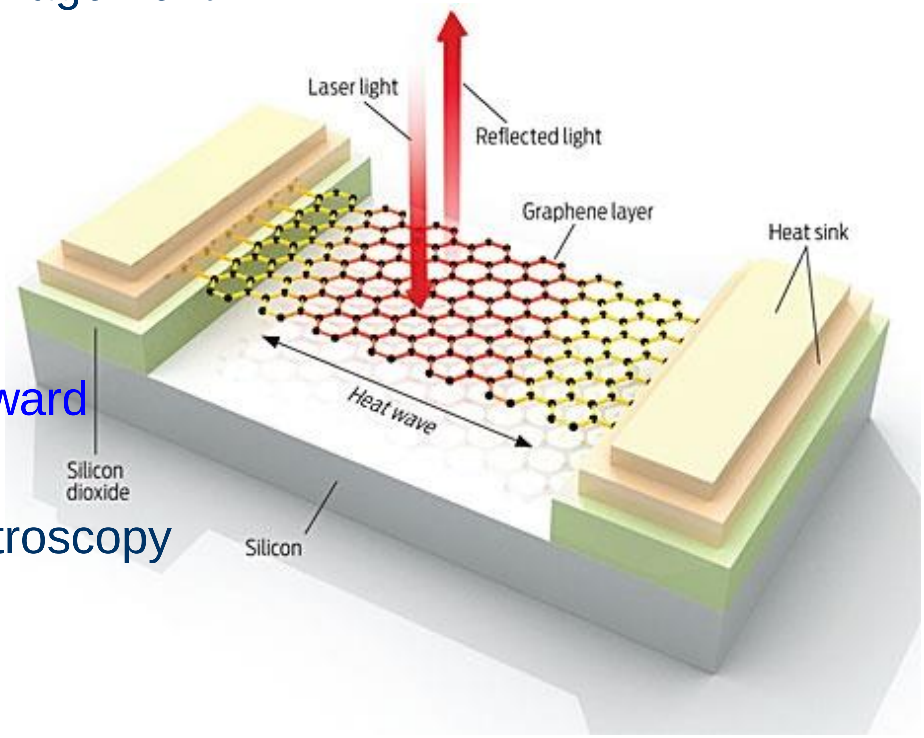

https://balandingroup.ucr.edu/

Funding Acknowledgement

National Science Foundation (NSF) program Designing Materials to Revolutionize and Engineer our Future (DMREF) via a project DMR-1921958 entitled Collaborative Research: Data Driven Discovery of Synthesis Pathways and Distinguishing Electronic Phenomena of 1D van der Waals Bonded Solids
UCR PI: A.A. Balandin, Co-PI: L. Bartels; Stanford Lead PI: E. Reed

Semiconductor Research Corporation (SRC) contract 2018-NM-2796 entitled One-Dimensional Single-Crystal van-der-Waals Metals: Ultimately-Downscaled Interconnects with Exceptional Current-Carrying Capacity and Reliability
UCR PI: A.A. Balandin, Co-PI: L. Bartels

Department of Energy (DOE) contract DE-SC0021020 Physical Mechanisms and Electric-Bias Control of Phase Transitions in Quasi-2D Charge-Density-Wave Quantum Materials
UCR PI: A.A. Balandin

NSF DMR Major Research Instrumentation (MRI): Development of a Cryogenic Integrated Micro-Raman-Brillouin-Mandelstam Spectrometer
UCR PI: A.A. Balandin, Co-PI: F. Kargar

Outline of the Talk

→ Definitions and Motivations: Quasi-1D and 2D van der Waals materials

→ Properties and applications of quasi-1D van der Waals materials

→ Current conduction of quasi-1D bundles
→ Electromagnetic interference shielding

→ Quasi-2D Charge-density-wave devices

→ Radiation hardness
→ Mechanism of switching
→ The “narrow band noise”

→ Conclusions

Materials Science

Physics

Electrical Engineering

Chemistry

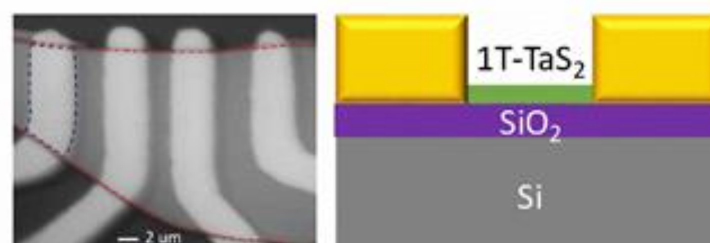

Terminology: Van der Waals Materials

Quasi-2D van der Waals Materials

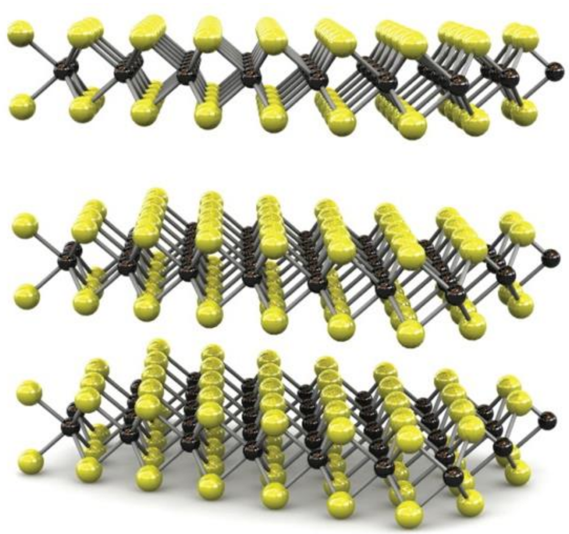

MoS_2

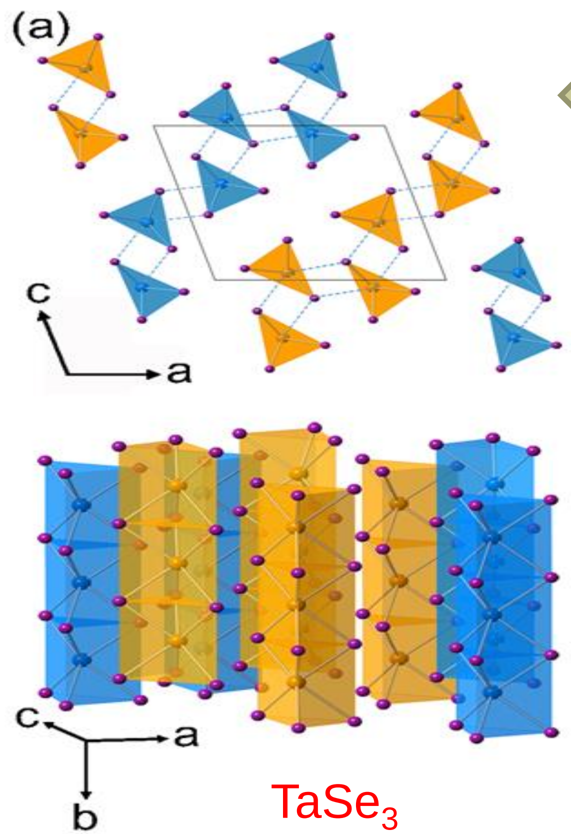

$TaSe_3$

atomic threads

Quasi-1D van der Waals Materials

→ Crystal structure of monoclinic $TaSe_3$, with alternating layers of $TaSe_3$

→ Cross section of the unit cell, perpendicular to the chain axis (b axis).

→ The side view: 1D nature of $TaSe_3$ chains along the b axis.

The Meaning of “Quasi” and “Quantum”

→“Quasi” in a sense of a bundle

→“Quasi” in a sense that you may have weaker covalent bonds in perpendicular plane

→ “Quantum” in a sense of quantum confinement: it can reveal itself differently for van der Waals materials

→ “Quantum” is relation to the charge-density-wave phases

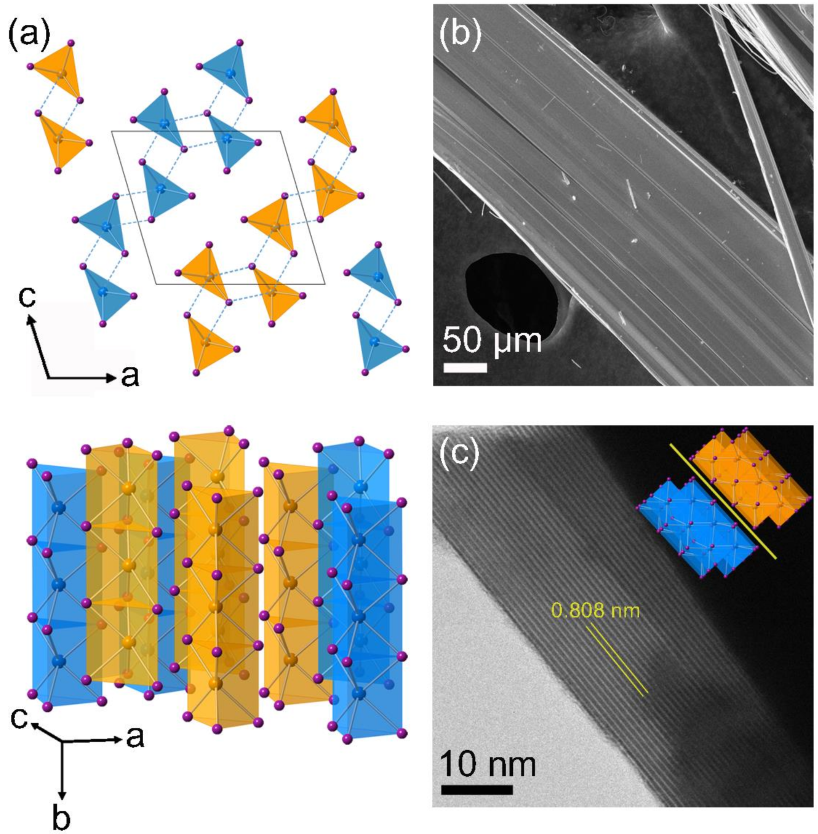

$TaSe_3$

Alexander A. Balandin, University of California - Riverside

Material Synthesis: Chemical Vapor Transport (CVT) or Chemical Vapor Deposition (CVD)

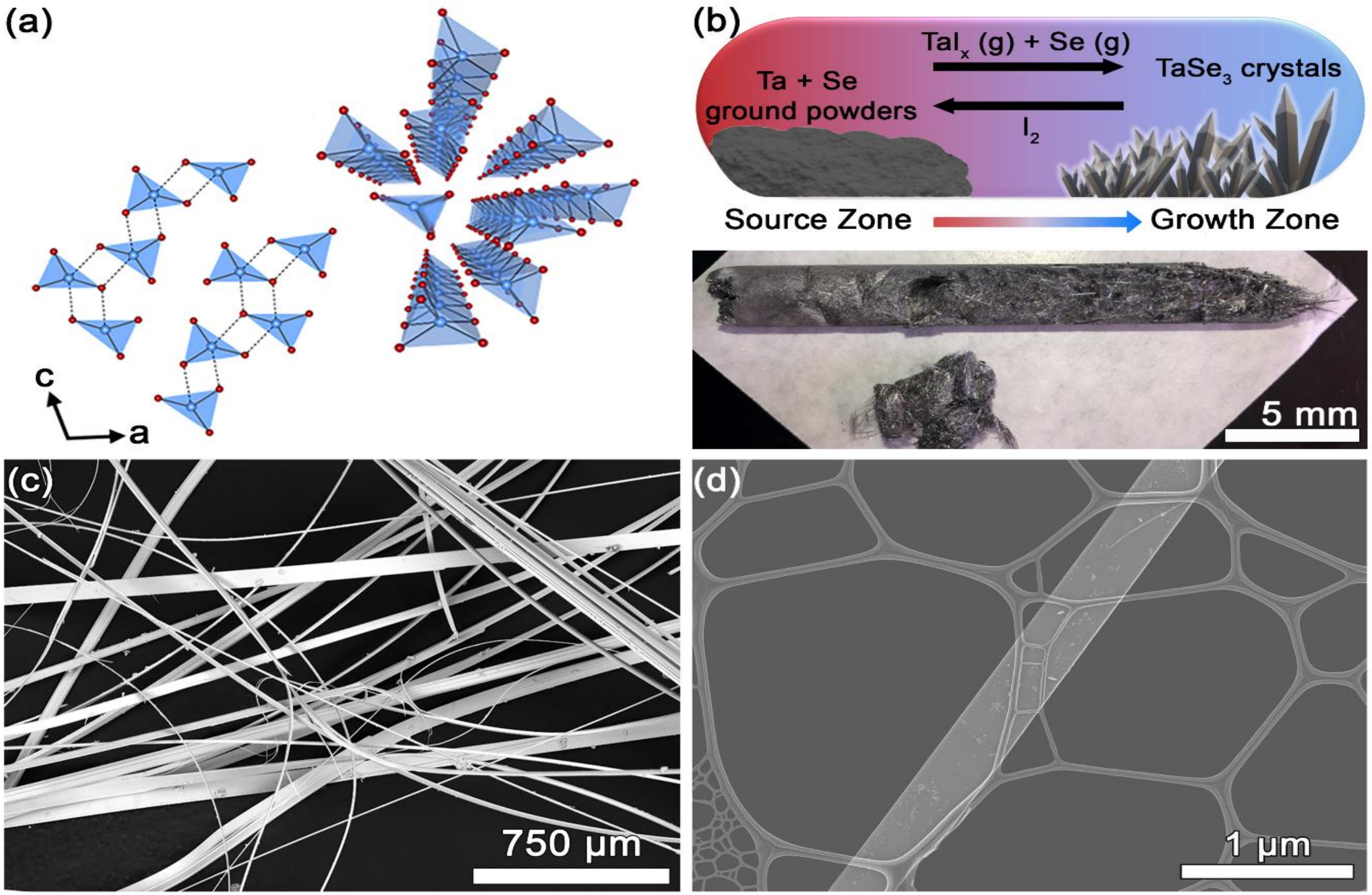

Z. Barani, et al., ACS Appl. Mater. Interfaces, 13, 21527 (2021).

Secondary electron image of a $TaSe_3$ nanowire produced by solvent exfoliation.

Fabrication of Quasi-1D and Quasi-2D Devices

E-Beam Lithography

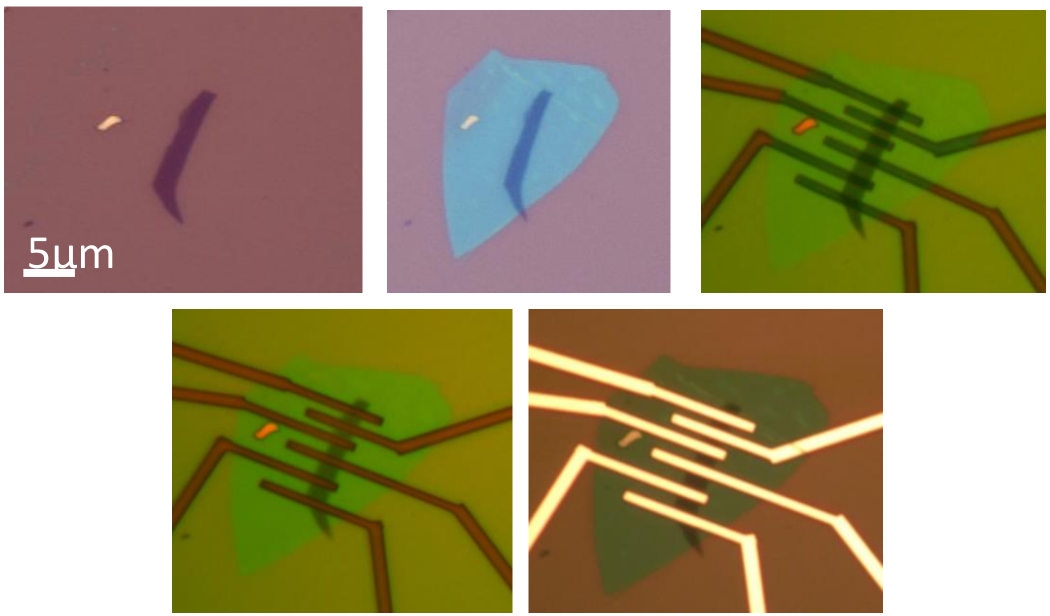

Shadow Mask Method

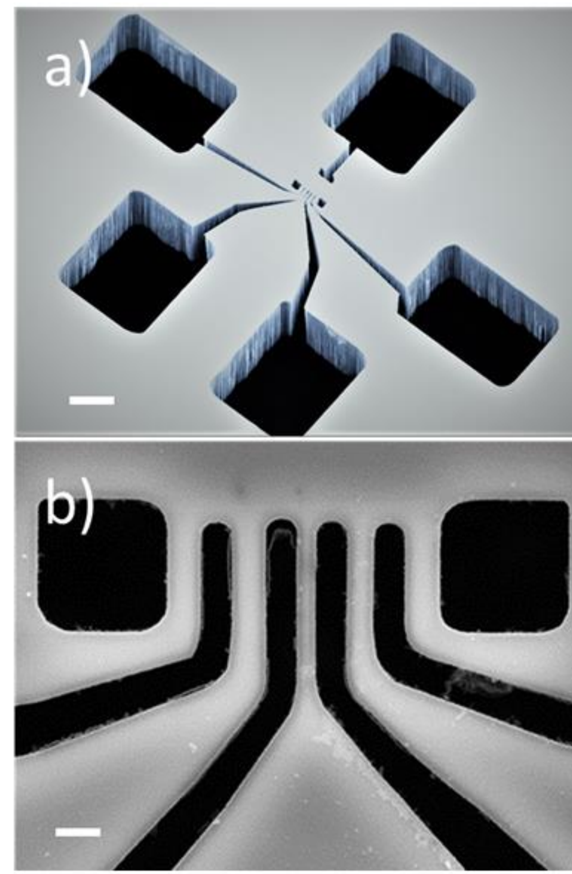

M. A. Stolyarov, et al., Nanoscale, 8, 15774 (2016).
A. Geremew, et al., IEEE Electron Device Lett., 39, 735 (2018).
A. Mohammadzadeh, et al., Appl. Phys. Lett., 118, 223101 (2021).

Quasi-1D Channel $TaSe_3$ Devices Fabricated by Electron Beam Lithography

Quasi-1D bundles and BN capping

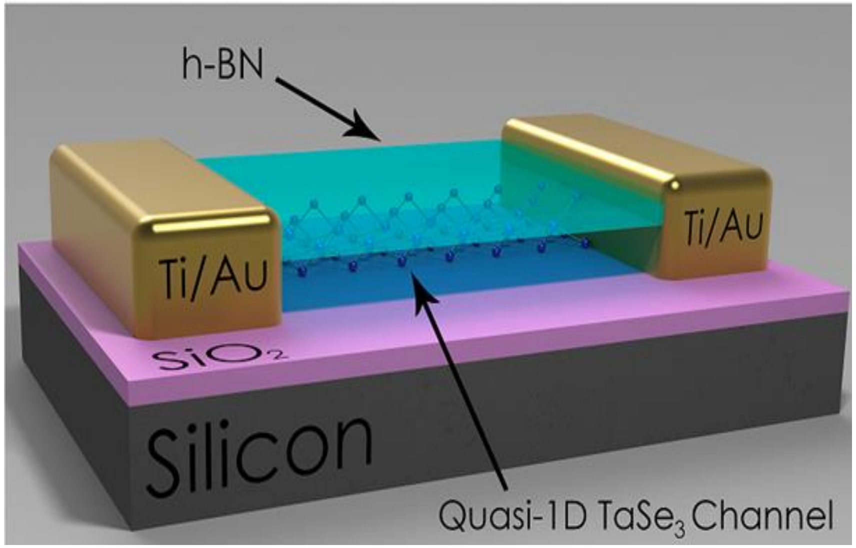

Schematic of the $TaSe_3$/h-BN quasi-1D / quasi-2D nanowire heterostructures used for the I-V testing.

$TaSe_3$ – metallic when it is stoichiometric and low defect concentration

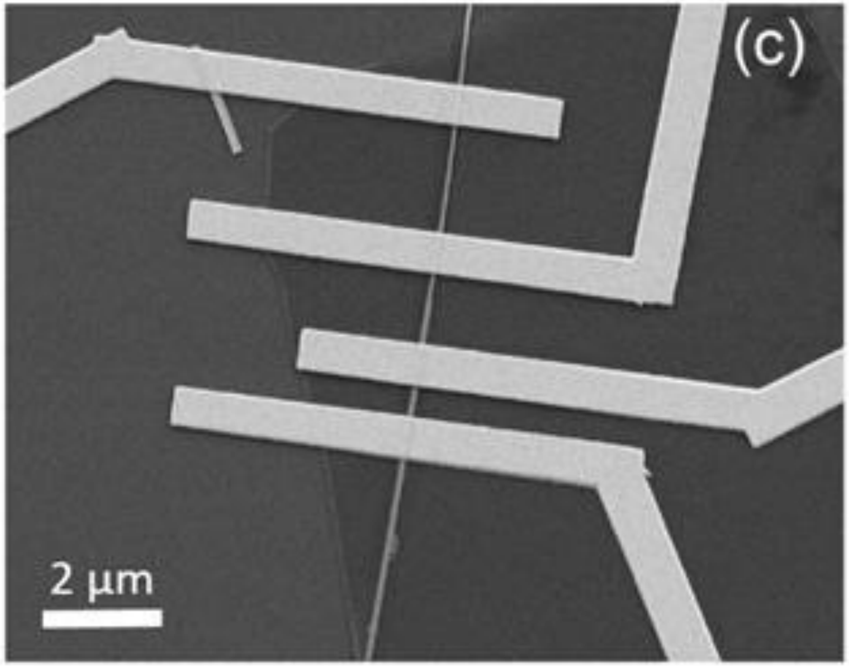

The metals tested for fabrication of Ohmic contacts included combinations of thin layers of Cr, Ti, Au, Pd together with a thicker Au layer.

Electrical Characteristics of Devices with Quasi-1D $TaSe_3$ Channels – Ohmic Contacts

→ Current-voltage characteristics of $TaSe_3$ devices with different channel length.

→ Linear characteristics at low voltage indicates good Ohmic contact of $TaSe_3$ channel with the metal electrodes.

The contact resistance extracted from TLM data is $2R_C$=22 Ω-μm

G. Liu, S. Rumyantsev, M. A. Bloodgood, T. T. Salguero, M. Shur, and A. A. Balandin, Nano Lett., 17, 377 (2017).

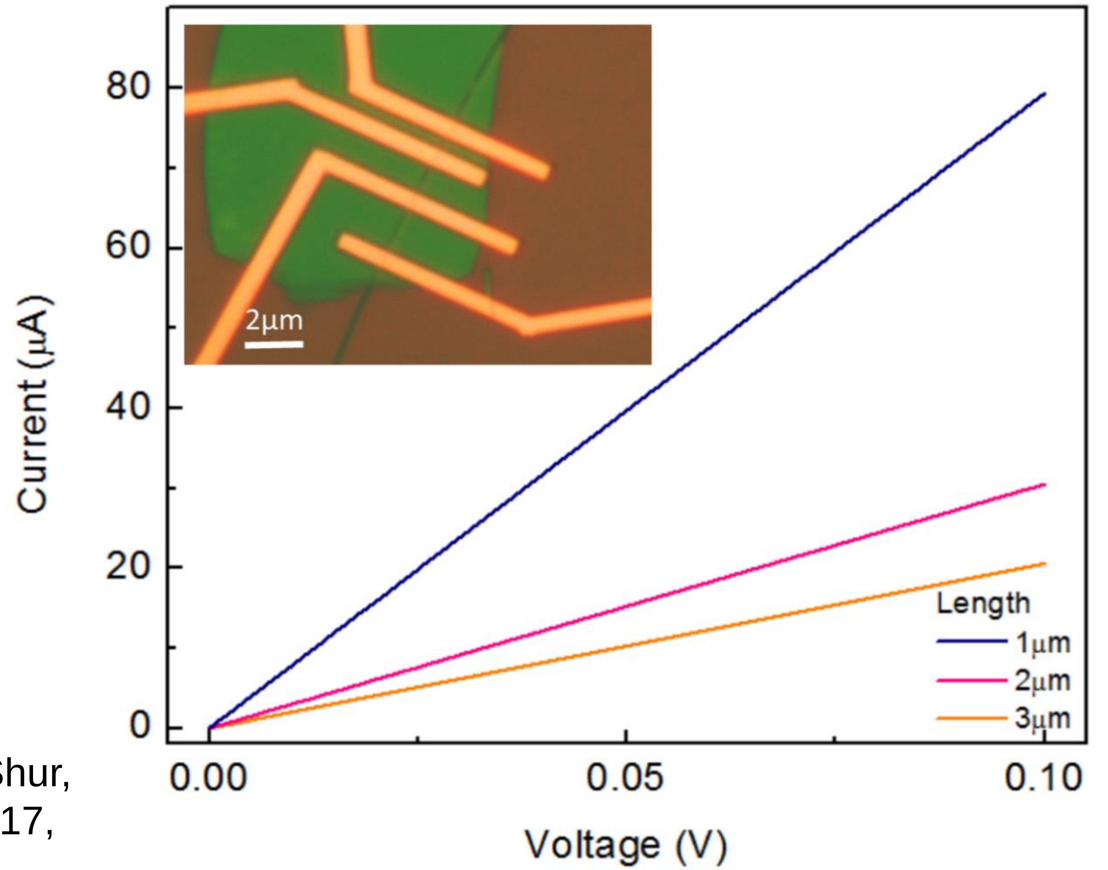

Current Density in Quasi-1D $TaSe_3$ Nanowires

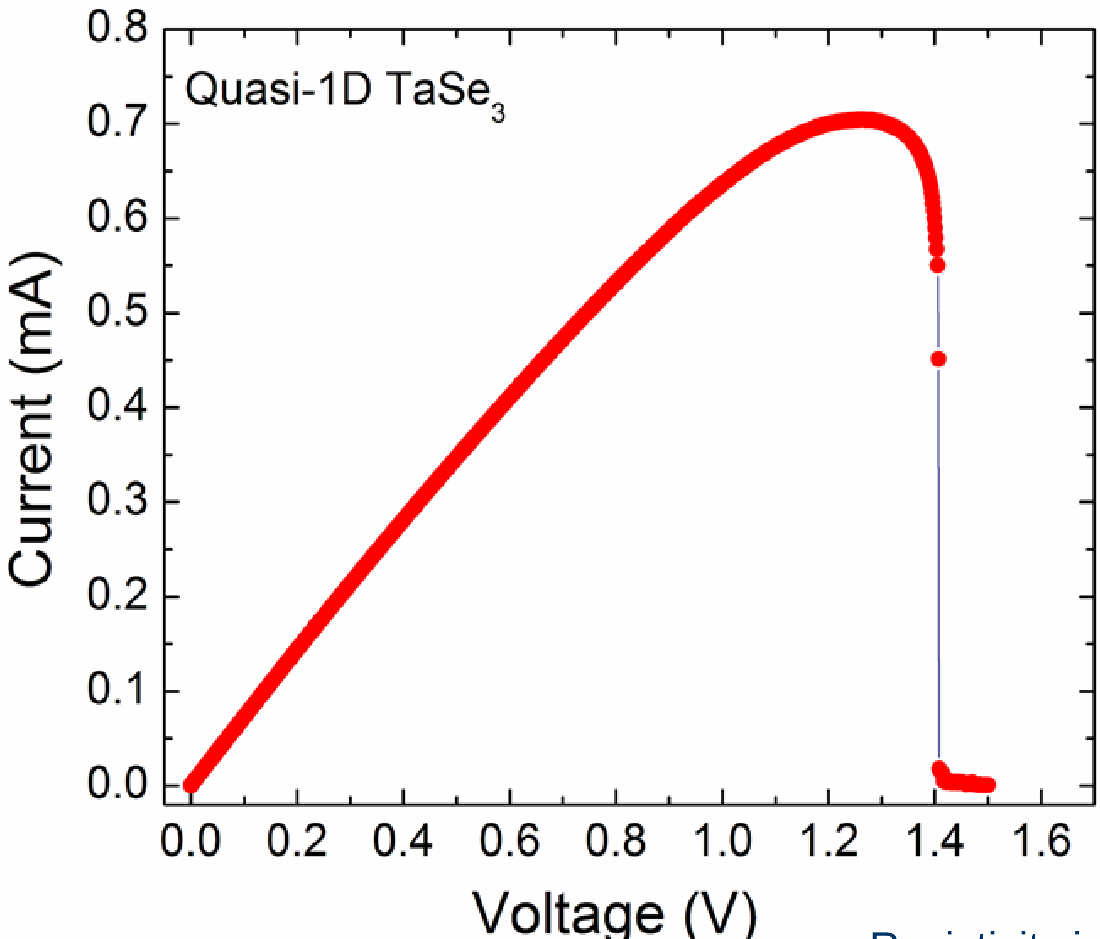

→ High-field I-V characteristics showing the breakdown point. In this specific device the breakdown is gradual.

→ Breakdown current density of about 32 MA/cm^2 — an order-of-magnitude higher than that for copper.

Nature of the breakdown – electromigration as established from the low-frequency noise studies.

Resistivity is $2.6 – 6.4\times10^{-4}$ Ω-cm.

Current Carrying Capacity of Quasi-1D $ZrTe_3$ van der Waals Nanoribbons

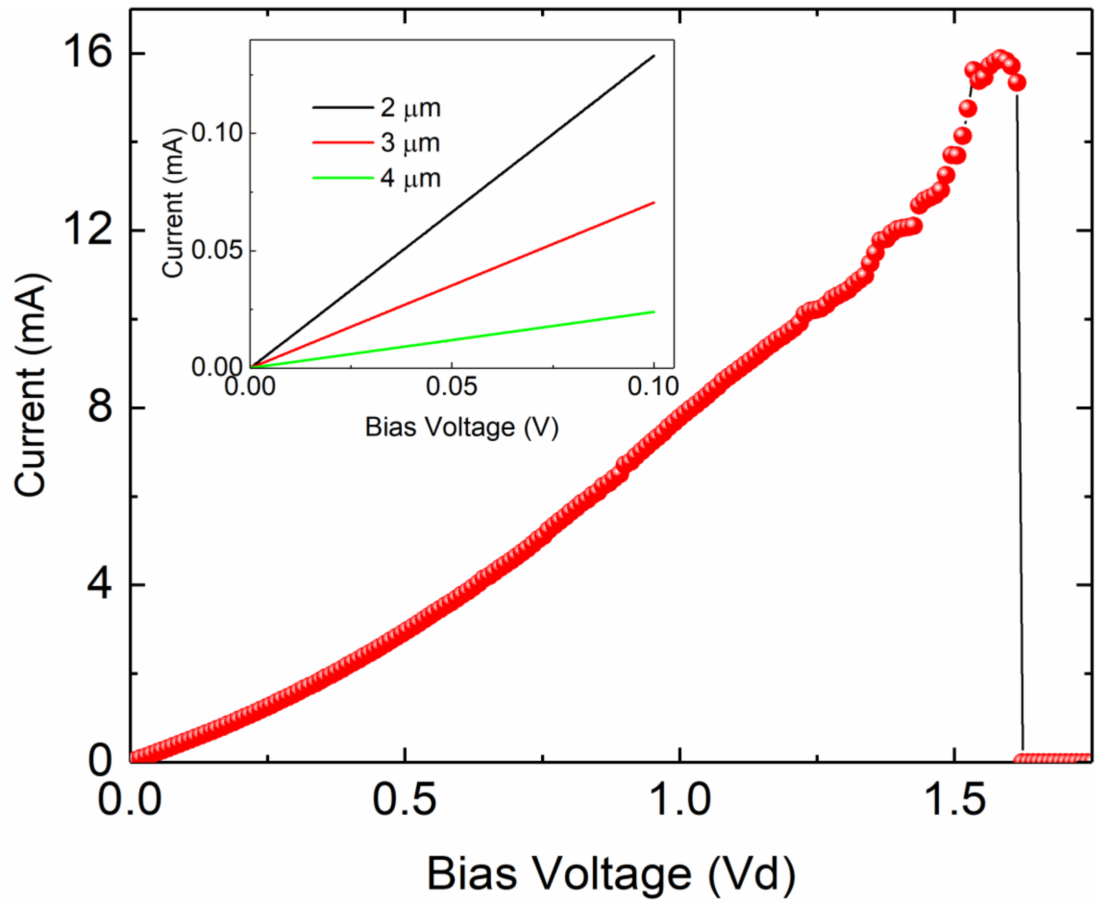

The breakdown current density, calculated with the AFM measured thickness and SEM measured width, corresponds to ~10^8 A/cm^2, reached at the voltage bias of ~1.6 V.

The inset shows low-field I-V characteristics of quasi-1D $ZrTe_3$ devices with different channel lengths.

A. Geremew, et al., "Current carrying capacity of quasi-1D $ZrTe_3$ van der Waals nanoribbons," IEEE Electron Device Lett., 39, 735 (2018).

Comparison with Copper Interconnects – Model Prediction

Conventional Elemental Metals

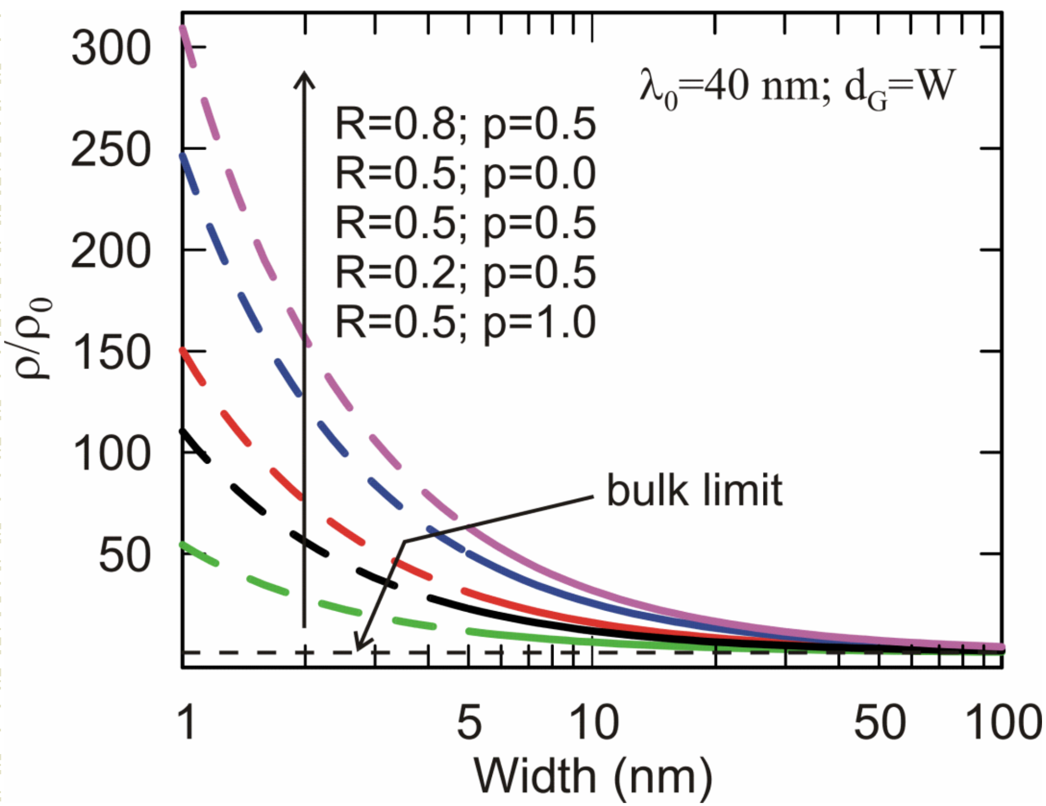

Resistivity trend from the Fuchs-Sondheimer model for the electron–nanowire surface scattering and the Mayadas-Shatzkes model for the electron–grain boundary scattering.

Electrical resistivity of Cu nanowires normalized to the bulk resistivity as a function of W.

Specularity parameters p defines electron scattering from nanowire surfaces; reflectivity R determines electron scattering from grain boundaries.

M. A. Stolyarov, et al., "Breakdown current density in h-BN-capped quasi-1D $TaSe_3$ metallic nanowires: prospects of interconnect applications," Nanoscale, 8, 15774 (2016).

Testing Prototype Interconnects Implemented with CVD Grown Quasi-1D Bundles of $TaSe_3$

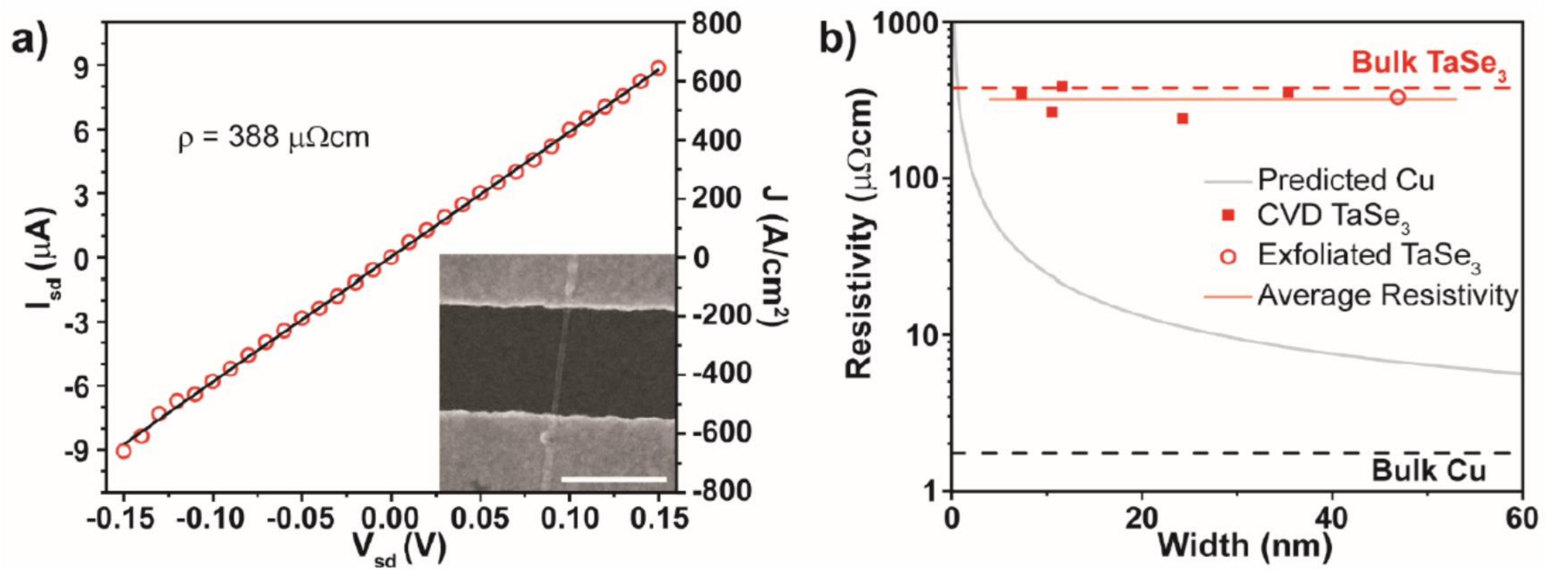

A.A. Balandin and L. Bartels, SRC – Intel Corporation: Task 2796.001 Fabrication and Testing of Quasi-1D van der Waals Metal Interconnects

T. A. Empante, et al., "Low resistivity and high breakdown current density of 10 nm diameter van der Waals $TaSe_3$ nanowires by chemical vapor deposition," Nano Letters 19, 4355 (2019).

One needs to find quasi-1D van der Waals material with low bulk resistivity → UCR – Stanford – NSF DMREF project on computational discovery of 1D materials.

Polymer Films with Quasi-1D van der Waals Materials

Chemical Exfoliation of CVT Material

→ Polymer composite films containing fillers comprised of quasi-1D van der Waals materials.
→ Fillers can exfoliation into bundles of *atomic threads.*
→ These nanostructures are characterized by extremely large aspect ratios of up to ~10^6.

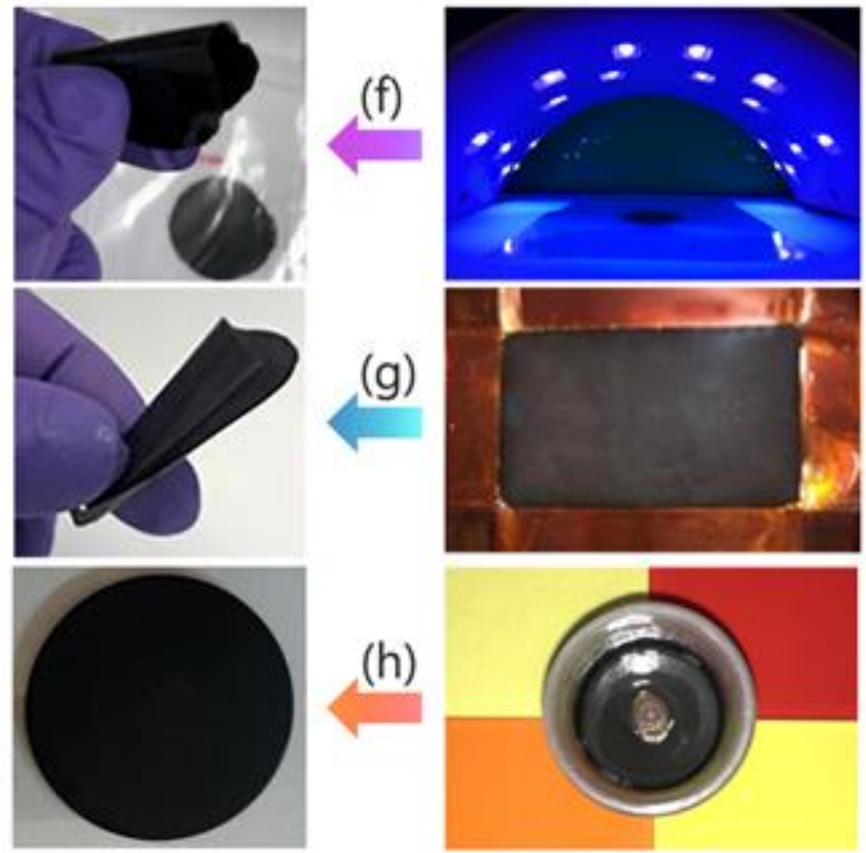

Quantum confinement works in different ways in 1D van der Waals materials

Electromagnetic Interference (EMI) Shielding – New Functionality

X-Band frequency range (8.2 GHz – 12.4 GHz)

(a)

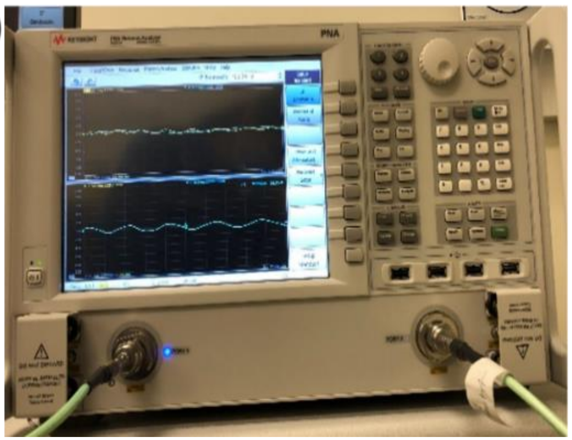

(b)

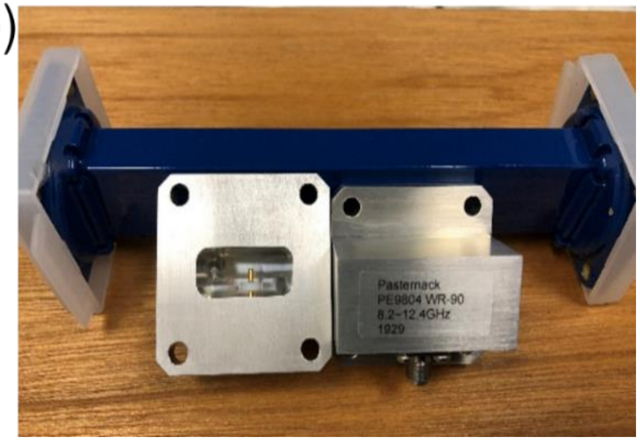

To determine EMI characteristics, we measured the scattering parameters, S_{ij}, using the two-port PNA system.

Extremely High Frequency (EHF) band (220 GHz – 320 GHz)

EMI shielding efficiency was determined from the measured scattering parameters using Agilent N5245A vector network analyzer (VNA) with a pair of frequency extenders

Z. Barani, et al., “Electrically insulating flexible films with quasi-1D van der Waals fillers as efficient electromagnetic shields in the GHz and sub-THz frequency bands” Advanced Materials, 33, 2007286 (2021).

EMI Shielding of Polymer Films with Quasi-1D Fillers in EHF Band

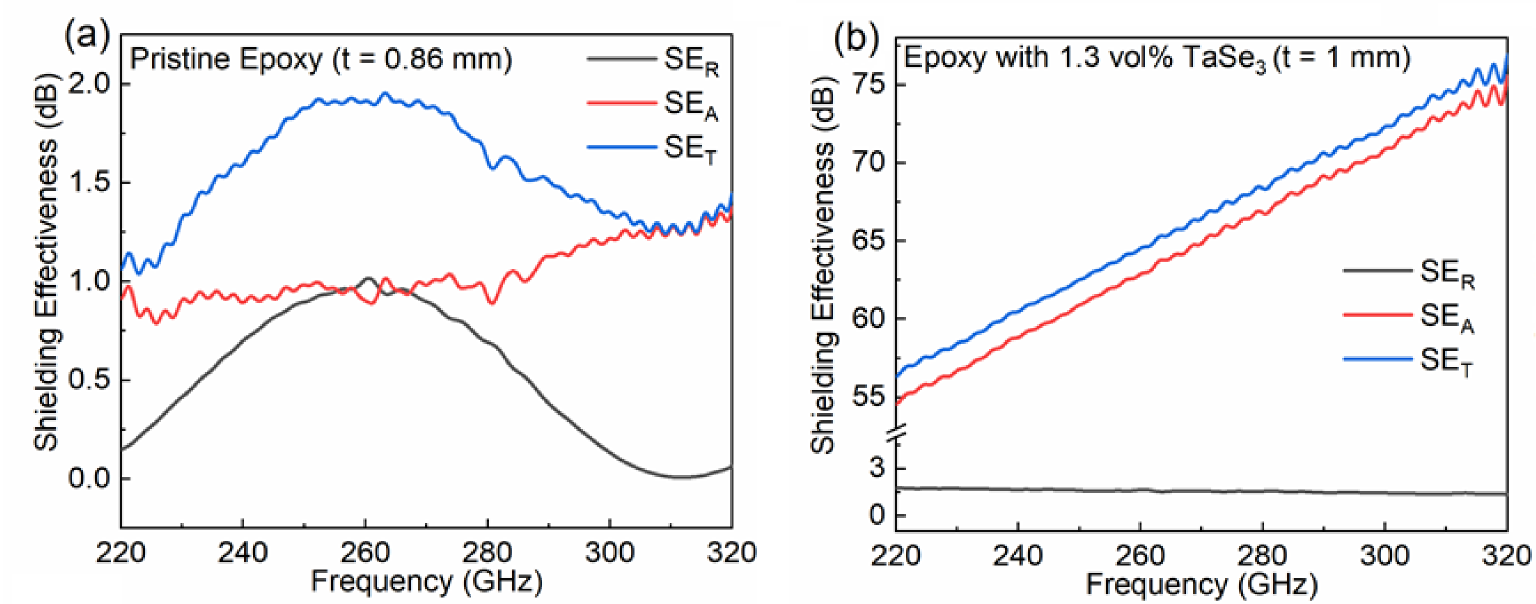

(a) Shielding effectiveness of pristine epoxy; (b) Reflection, absorption, and total shielding effectiveness.

→ Note that absorption is the dominant mechanism in blocking the EM waves in EHF band.

→ The films are electrically insulating: local EM coupling to the quasi-1D nanowires

Z. Barani, et al., “Electrically insulating flexible films with quasi-1D van der Waals fillers as efficient electromagnetic shields in the GHz and sub-THz frequency bands” Advanced Materials, 33, 2007286 (2021).

| Nano-Device Laboratory >

EM-Polarization Selective Composites with Quasi-1D van der Waals Metallic Fillers

Aligned fillers of quasi-1D metals

Quasi-1D materials are building blocks for new functionality

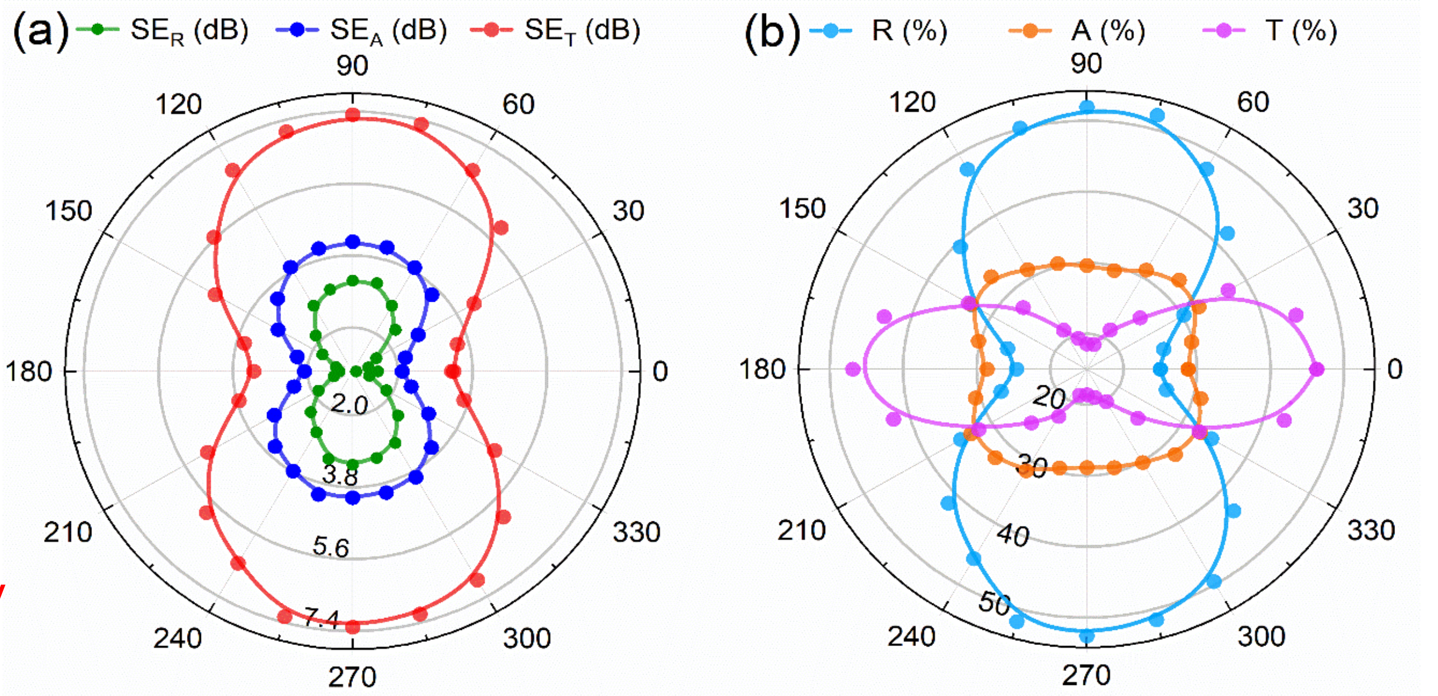

Angular dependency of (a) the reflection, absorption, and total shielding effectiveness, and (b) reflection absorption, and transmission coefficients of sample D with 1.61 vol% aligned quasi-1D $TaSe_3$ fillers. As shown in (b) the reflection is highly correlated with sample orientation whereas absorption varies weakly.

Z. Barani, et al., ACS Appl. Mater. Interfaces, 13, 21527 (2021).

Electronic Devices Printed with Inks of Quasi-1D van der Waals Materials

TiS_3 is a semiconductor

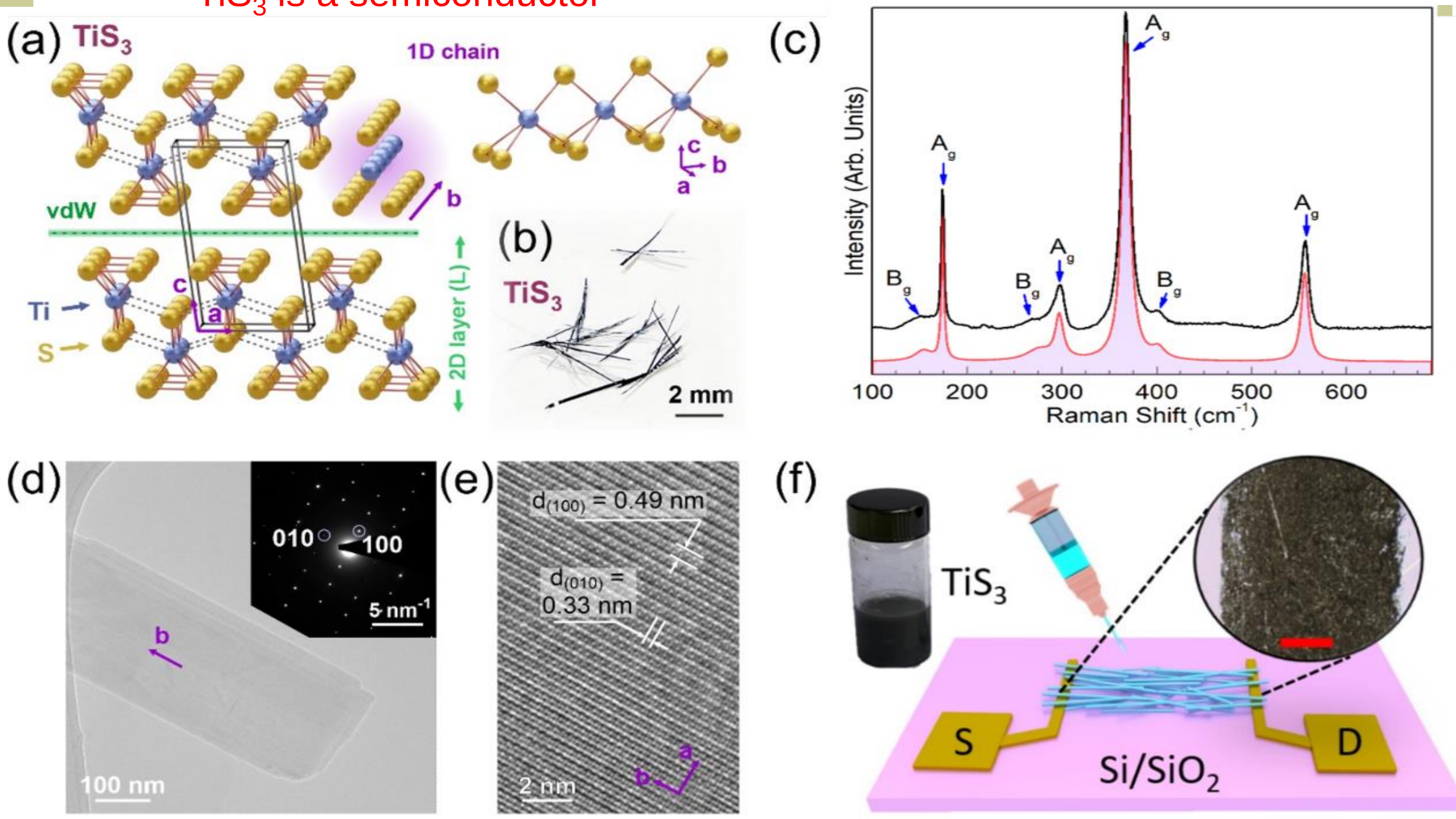

S. Baragani, et al., "Printed Electronic Devices with Inks of TiS_3 Quasi-One-Dimensional van der Waals Material", ACS Appl. Mater. Interfaces (2021).

Charge Density Waves: Quasi-1D Crystals

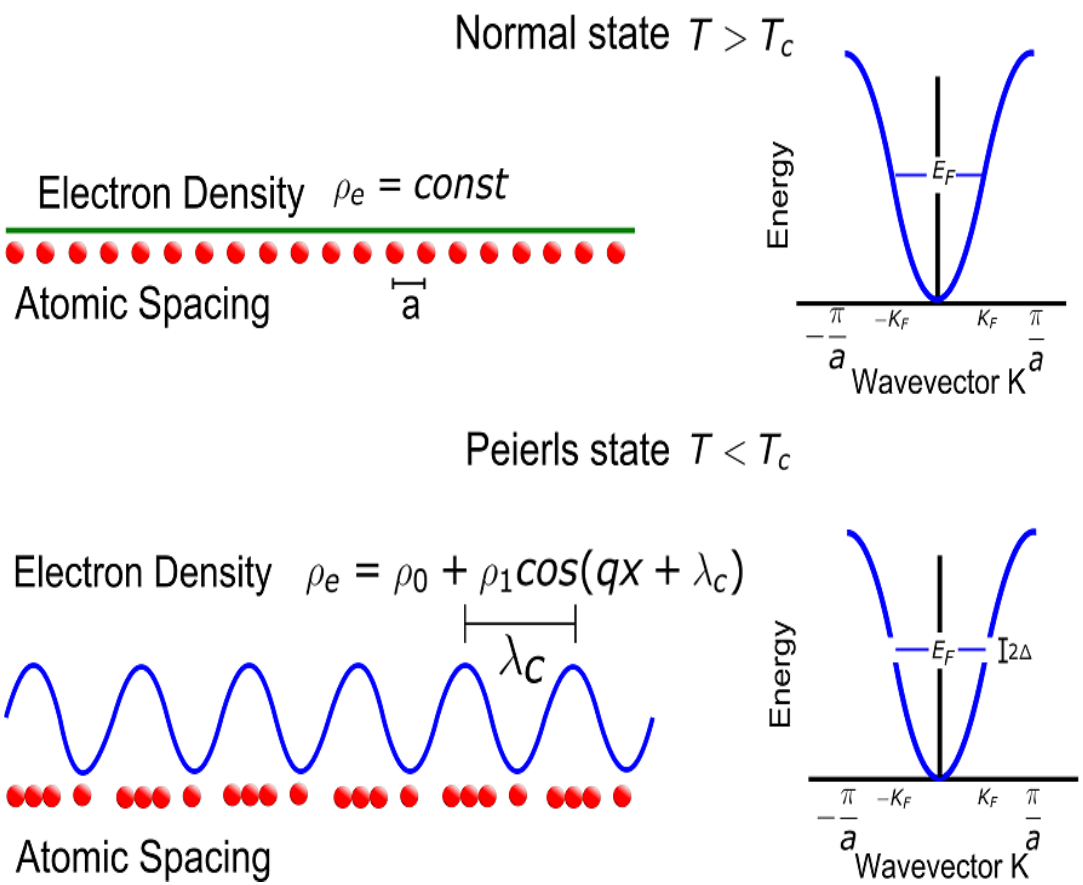

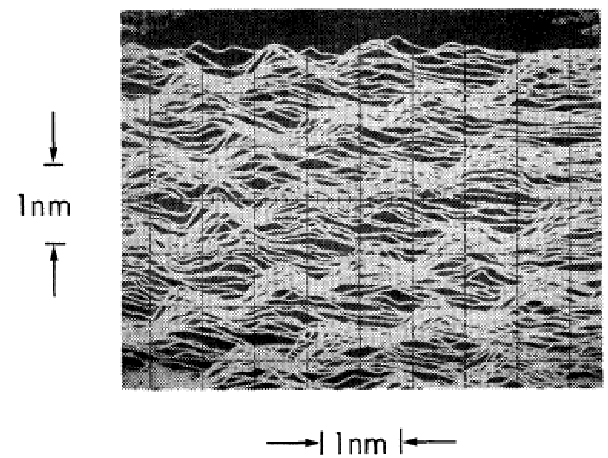

R.V. Coleman, *Phys. Rev. Lett.*, **55**, 394 (1985).

Macroscopic quantum phenomena: coherence length >1 μm

Quantum materials

Depinning and Sliding of CDWs in Bulk Quasi-1D CDW Materials

CDWs in metallic crystals form due to the wave nature of electrons – a manifestation of quantum mechanical wave nature of electrons – causing the electronic charge density to become spatially modulated.

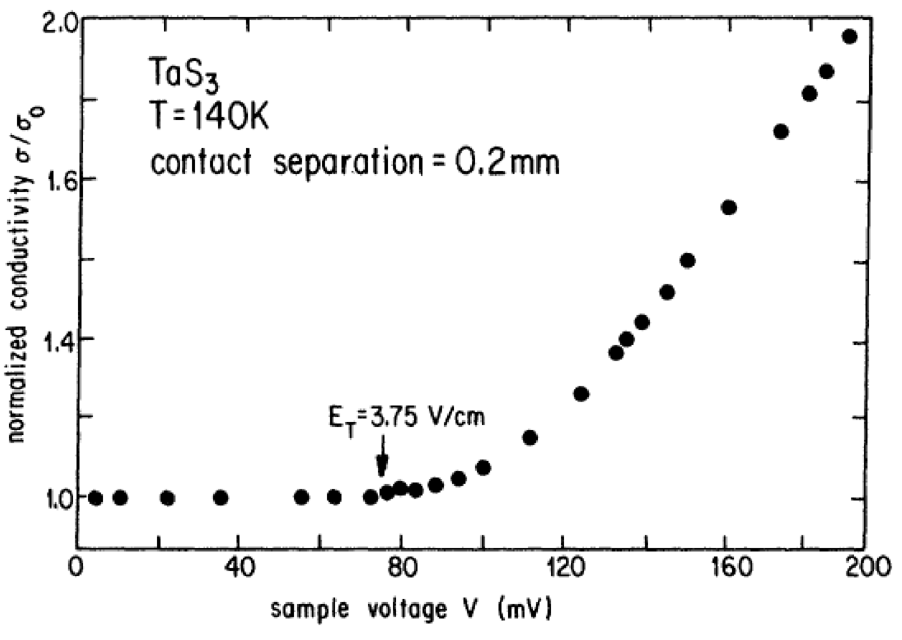

G. Gruner, et al., Phys. Rev. B, 23, 6813 (1981).

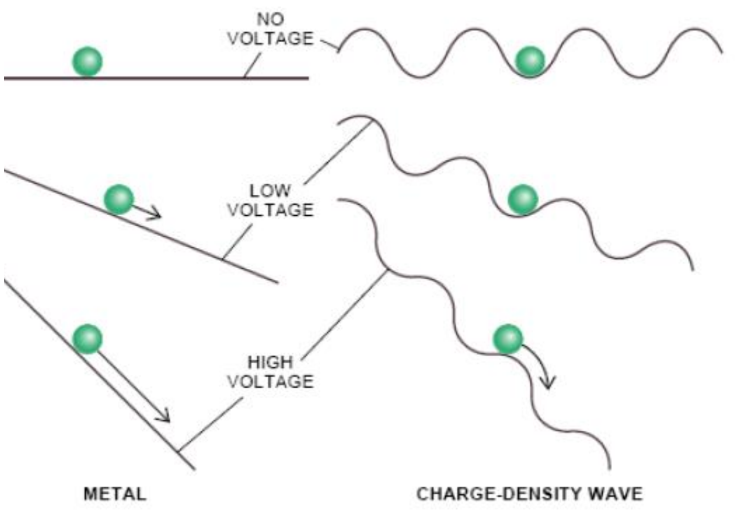

For fields larger than a threshold field E_T, the sliding CDW provides a second conduction path next to a single-particle electron conduction. Macroscopically this leads to non-linear electrical conductivity and oscillations for large fields.

Other Examples of Current Oscillations in Bulk Quasi-1D CDW Materials

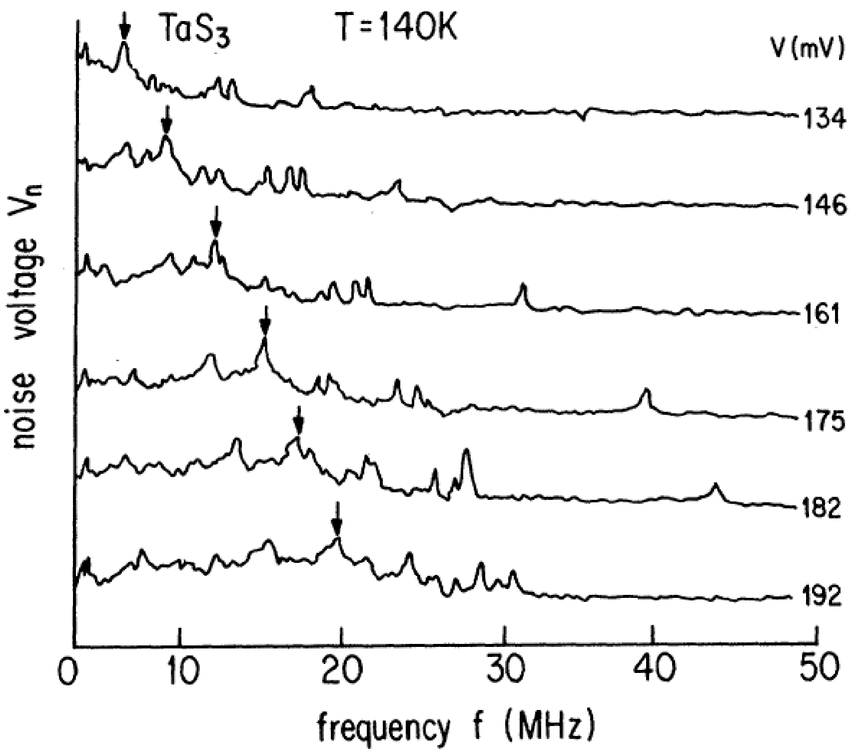

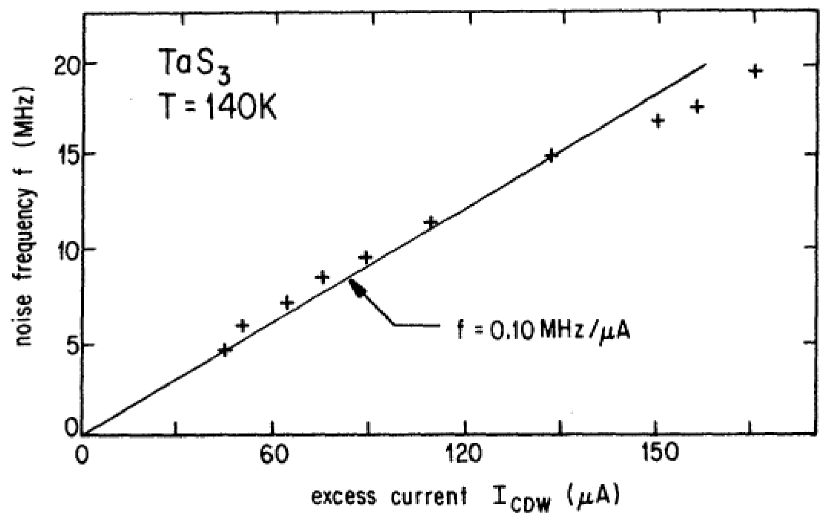

G. Gruner, et al., Phys. Rev. B, 23, 6813 (1981).

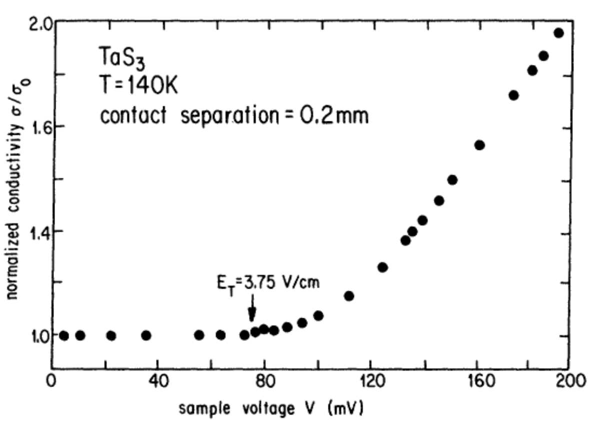

Rebirth of the Field of CDW Materials: Quasi-2D Films of 1T-TaS_2

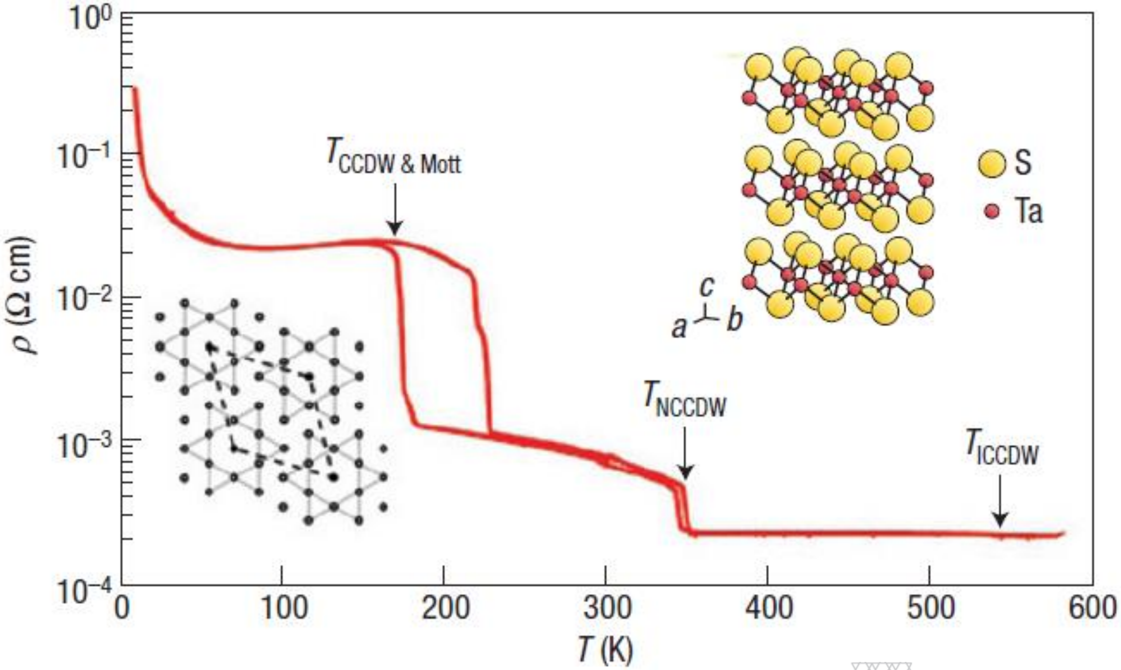

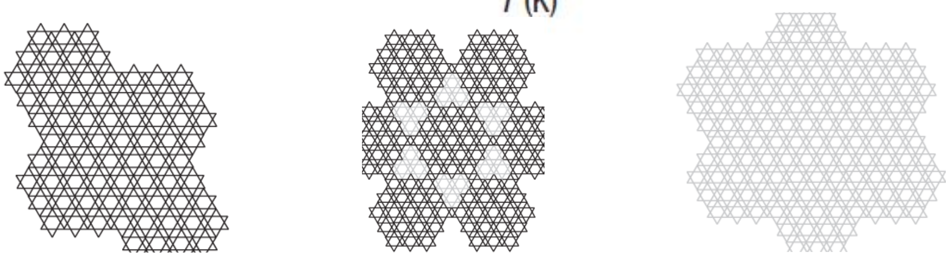

1D → 2D

Ambient-pressure phases of 1T-TaS_2. The phases are: a metallic phase at temperatures above 550 K; an IC-CDW phase above 350 K; an NC-CDW phase above 190 K; a C-CDW Mott phase below 190 K. Also shown are the Ta atom distortions in the fully commensurate phase and the crystal structure of 1T-TaS_2.

B. Sipos, et al., Nature Mater., 7, 960 (2008).

There are multiple phase transition points – some of them are above RT

Two-Terminal CDW Quasi-2D 1T-TaS_2 Devices

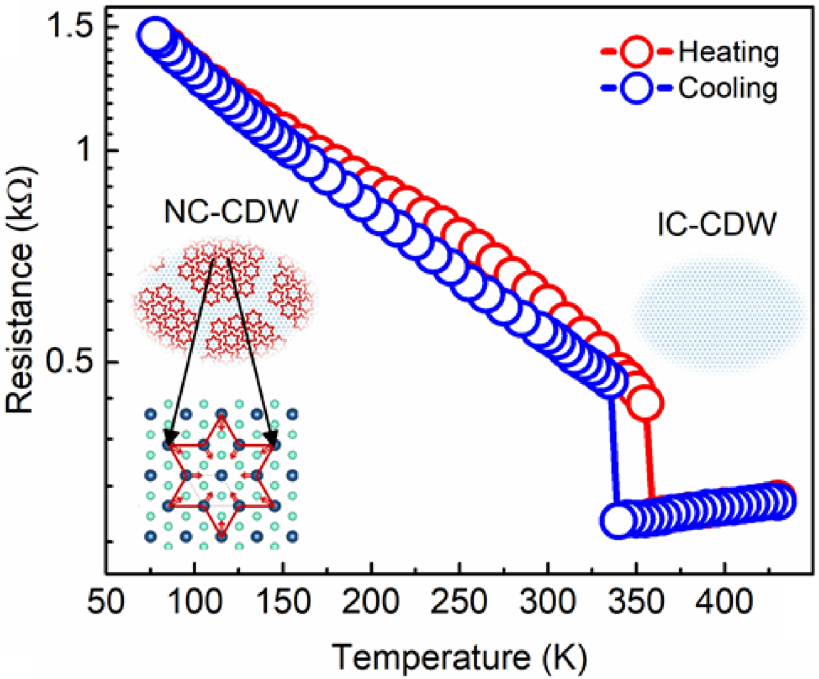

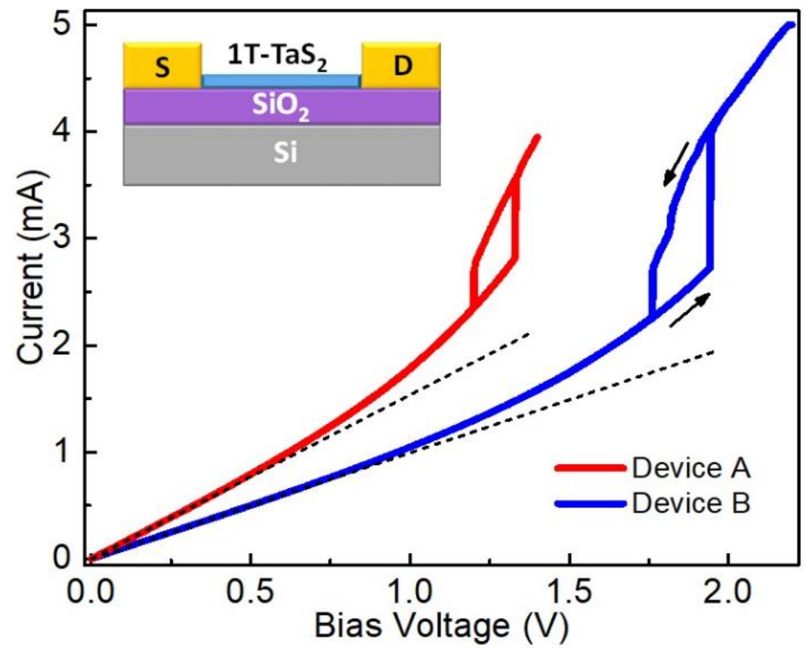

→ NC-CDW -- IC-CDW transition can be induced by changing the temperature or passing electrical current

→ Use NC-CDW – IC-CDW transition instead of depinning and sliding

→ NOT another resistive switch

The First Room Temperature CDW Device

Idea: utilize NC-CDW–IC-CDW transition at 350 K

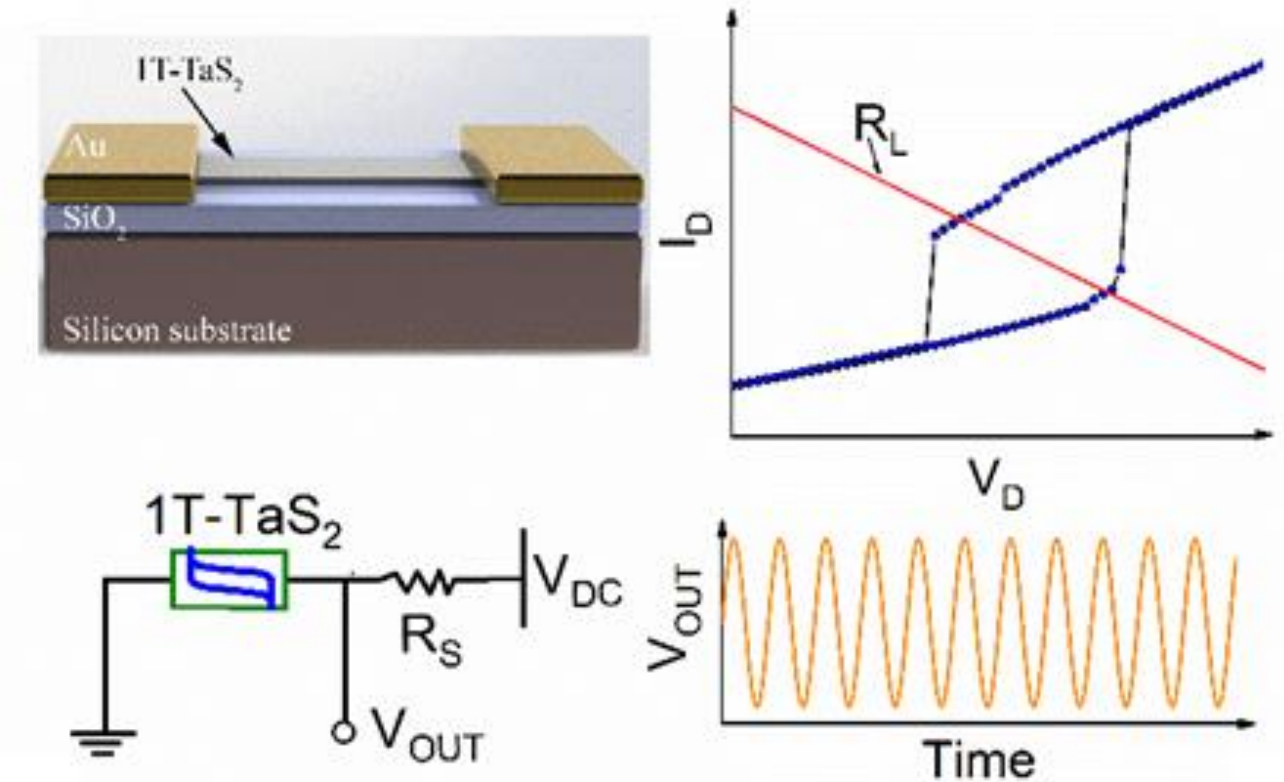

A switch that is not a transistor

This is not a resistive switching

CDW device can be low power and fast

I-V Characteristics of Thin Film 1T-TaS_2

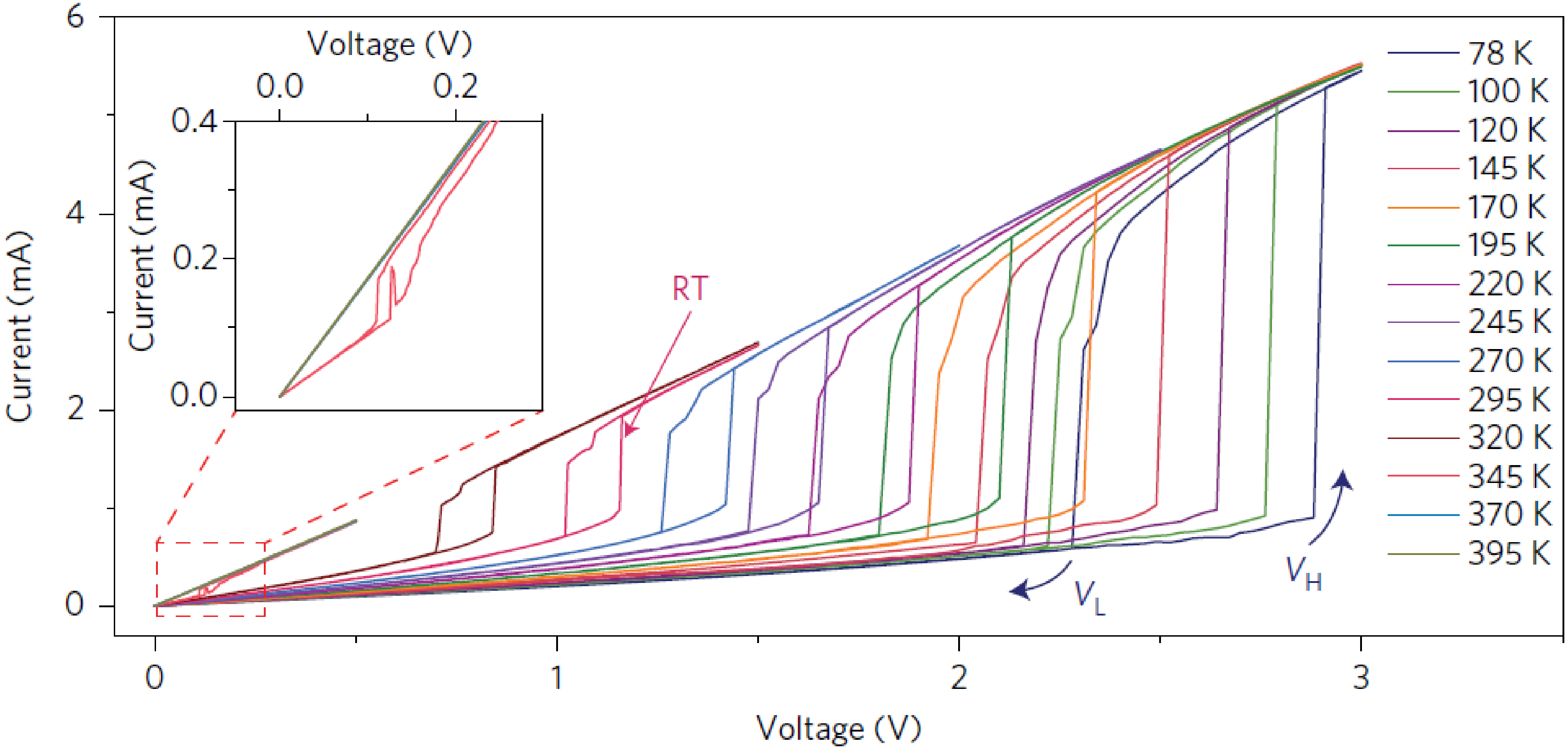

The threshold switching effect is prominent from 78 K to 320 K. The blues arrows indicate the voltage sweep direction for the measurement at 78 K. For all the other temperatures, V_H is always higher than V_L. The switching is prominent up to 320 K, and becomes less pronounced as the temperature approaches the NC-CDW–IC-CDW transition at 350 K. As shown in the inset, at 345 K (red curve), the switching is still measurable.

G. Liu, B. Debnath, T. T. Salguero, R. K. Lake, and A. A. Balandin, Nature Nano, 11, 845 (2016).

Oscillator Based on 1T-TaS_2 Device

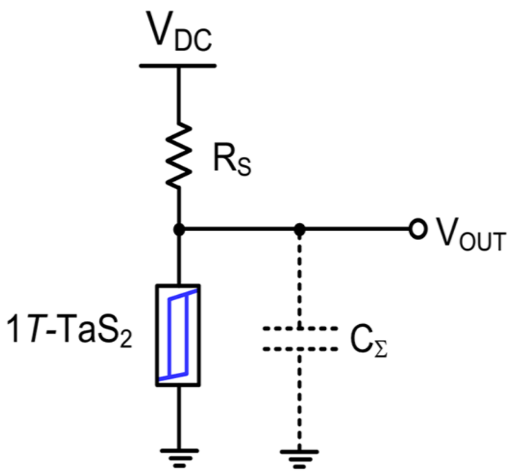

Different operation mechanism from early devices – no de-pinning

Allows for high T operation

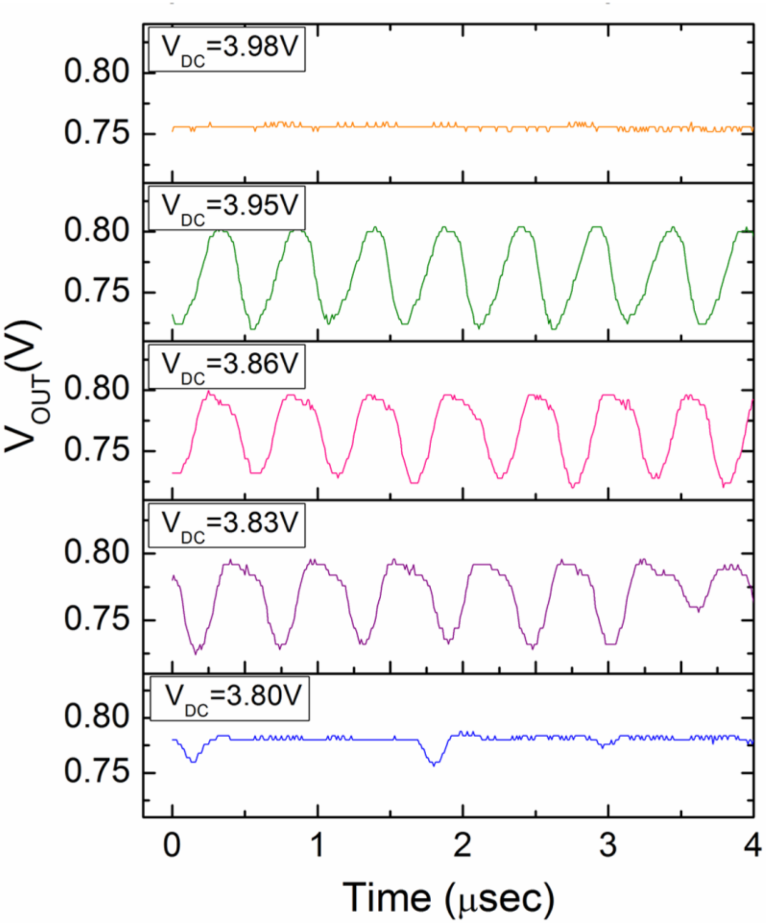

→Circuit schematic of the oscillator consists of the 1T-TaS_2 film, a series connected load resistor, and a lumped capacitance from the output node to ground. The load resistance is 1 kΩ.

→Voltage oscillations under different V_{DC}. The circuit oscillates when V_{DC} is within the range of 3.83-3.95 V. The frequency is 1.77 MHz, 1.85 MHz, and 2 MHz when V_{DC} is 3.83, 3.86 and 3.95 V, respectively.

An Integrated 1T-TaS_2 – h-BN – Graphene Oscillator

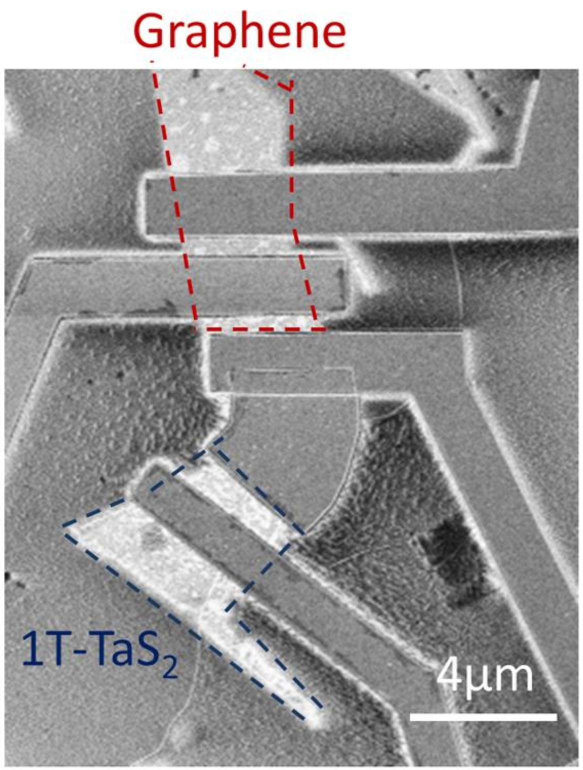

The SEM image of the integrated 1T-TaS_2–BN–graphene voltage controlled oscillator. The graphene and the TaS_2 are highlighted by dashed lines.

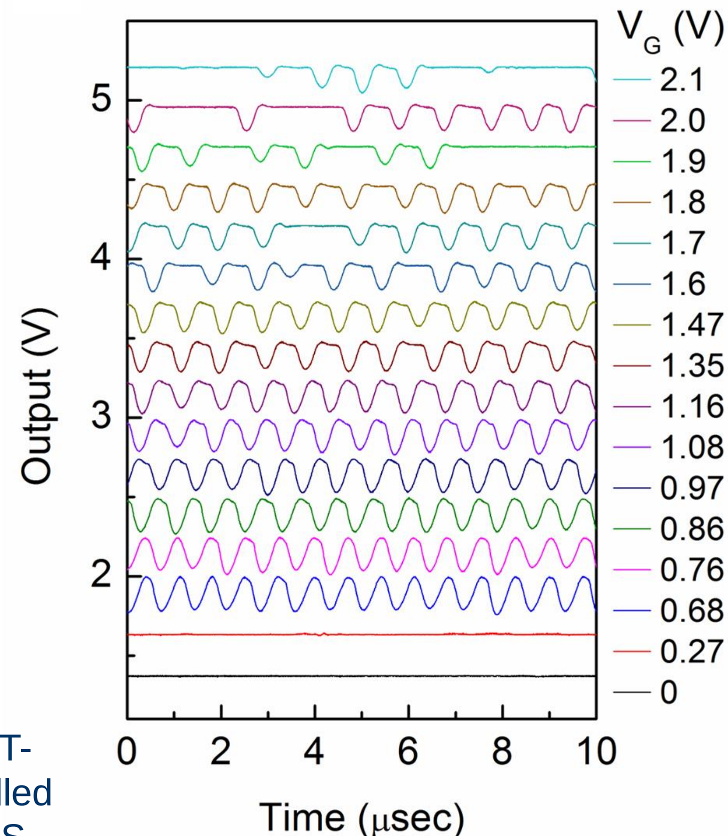

Output waveforms at different gate biases when V_{DC} is fixed at 3.65 V. The oscillation frequency is tunable with gate biases in the range of 0.68 V to 1.8 V. The different waveforms are vertically offset of 0.25 V for clarity.

G. Liu, B. Debnath, T. T. Salguero, R. K. Lake, and A. A. Balandin, Nature Nano, 11, 845 (2016).

1T-TaS_2 – h-BN – Graphene CDW VCO

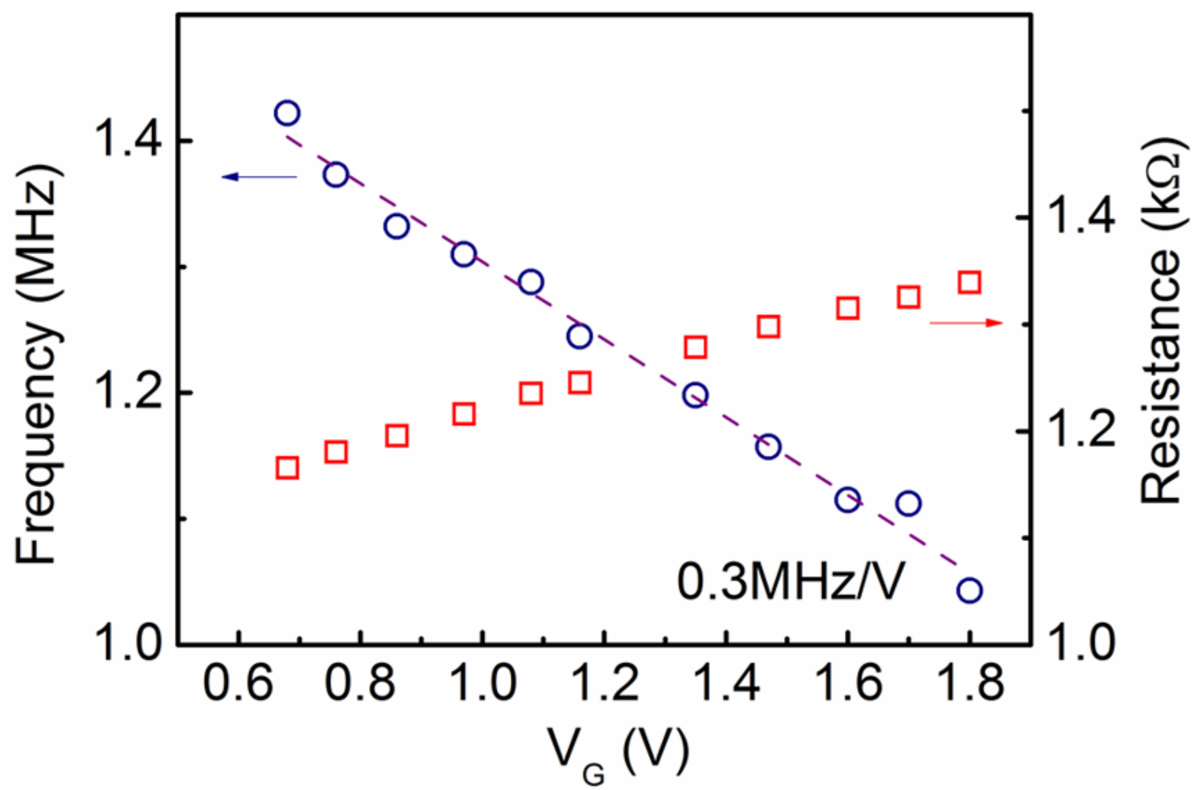

The dependence of oscillation frequency as function of gate bias.

Blue circles show the frequency of the oscillation under increased gate bias. The frequency can be adjusted monotonically with the tuning sensitivity of 0.3M Hz/V.

The red squares are the resistance value of the G-FET under different gate biases with fixed V_{DC}=2.4V.

G. Liu, B. Debnath, T. R. Pope, T. T. Salguero, R. K. Lake, and A. A. Balandin, Nature Nano, 11, 845 (2016).

1T-TaS_2 CDW Devices Under X-Ray Irradiation

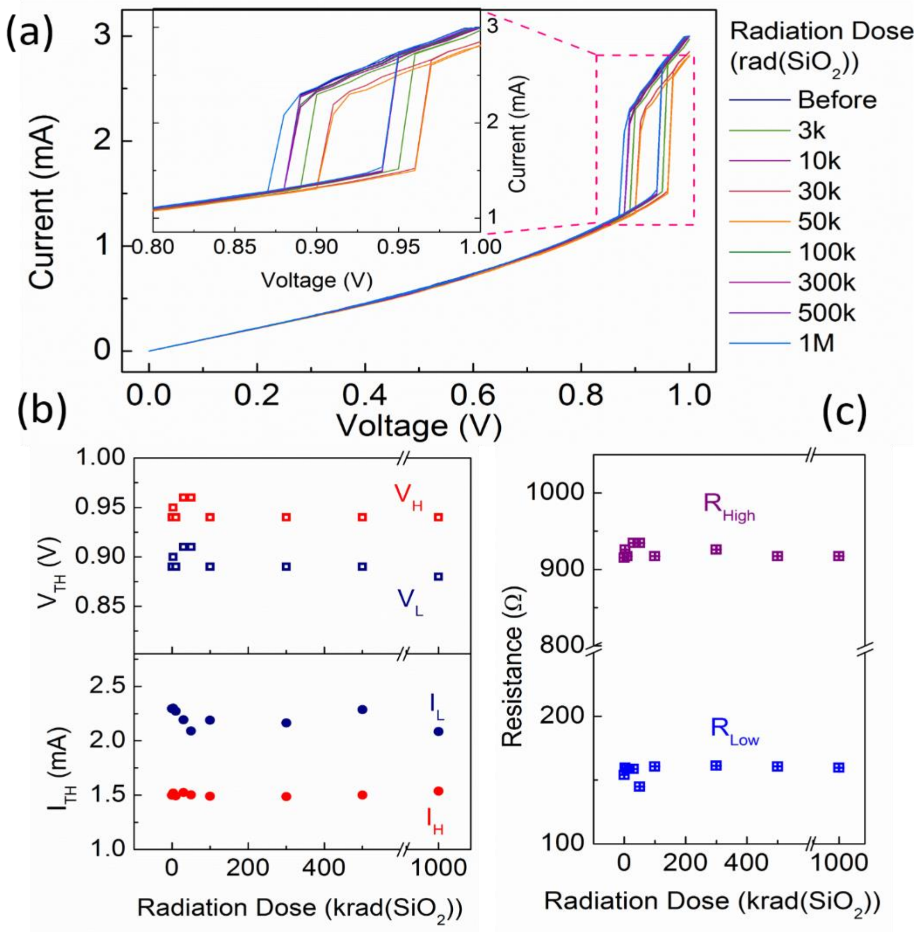

TID response of 1T-TaS_2 devices up to 1 M rad (SiO_2). (a) I-V curves measured after each X-ray irradiation step. (b) Threshold voltages, V_H and V_L, threshold currents, I_H and I_L as function of dose. (c) Extracted resistance at the high resistance and low resistance states as a function of dose.

Carrier concentration:
10^{21} cm^{-2} - 10^{22} cm^{-2}

G. Liu, E. X. Zhang, C. Liang, M. Bloodgood, T. Salguero, D. Fleetwood, A. A. Balandin, “Total-ionizing-dose effects on threshold switching in 1T-TaS_2 charge density wave devices,” IEEE Electron Device Letters, 38, 1724 (2017).

Radiation Hardness of CDW Devices

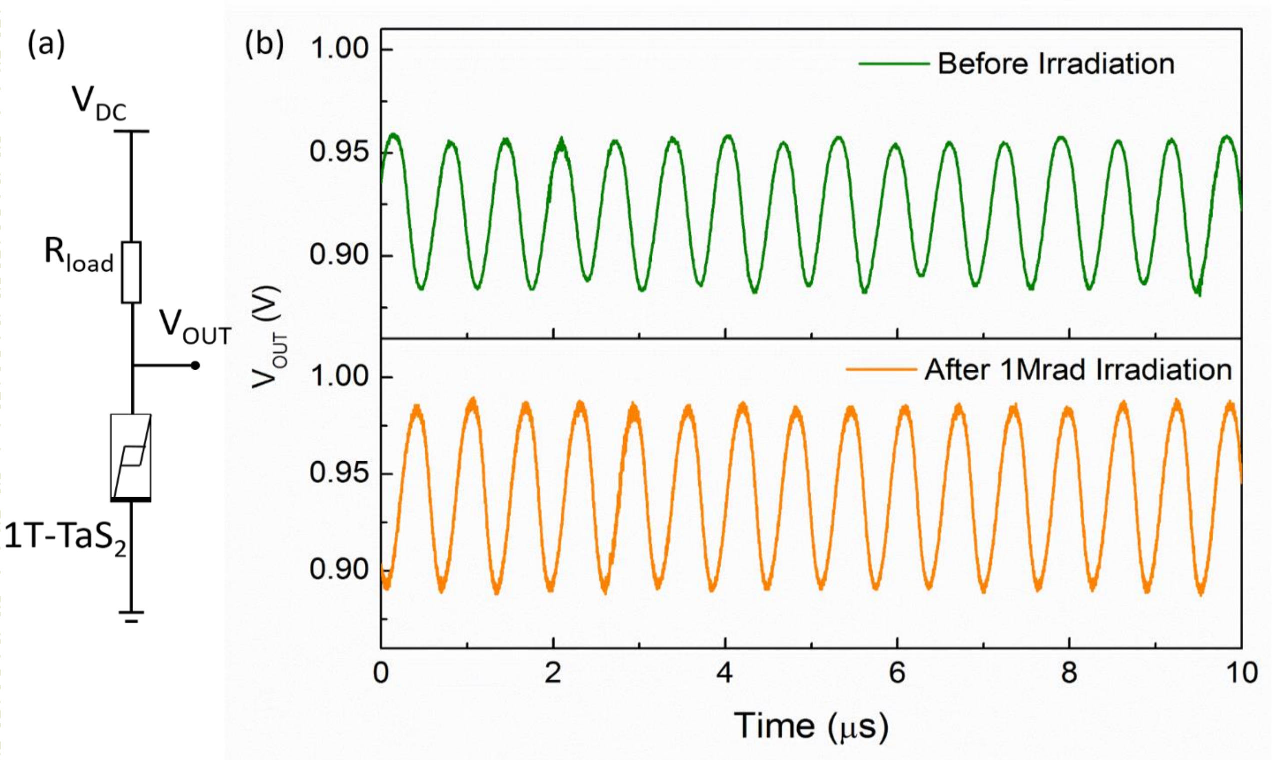

(a) Circuit schematic diagram of a self-sustaining oscillator implemented with one $1T\text{-}TaS_2$ device and a load resistor.

(a) Oscillation waveform before and after 1 Mrad(SiO_2) X-ray irradiation

G. Liu, E. X. Zhang, C. Liang, M. Bloodgood, T. Salguero, D. Fleetwood, A. A. Balandin, "Total-ionizing-dose effects on threshold switching in $1T\text{-}TaS_2$ charge density wave devices," IEEE Electron Device Letters, 38, 1724 (2017).

Proton Bombardment Immune Devices Based on CDW Transition in 1T-TaS_2

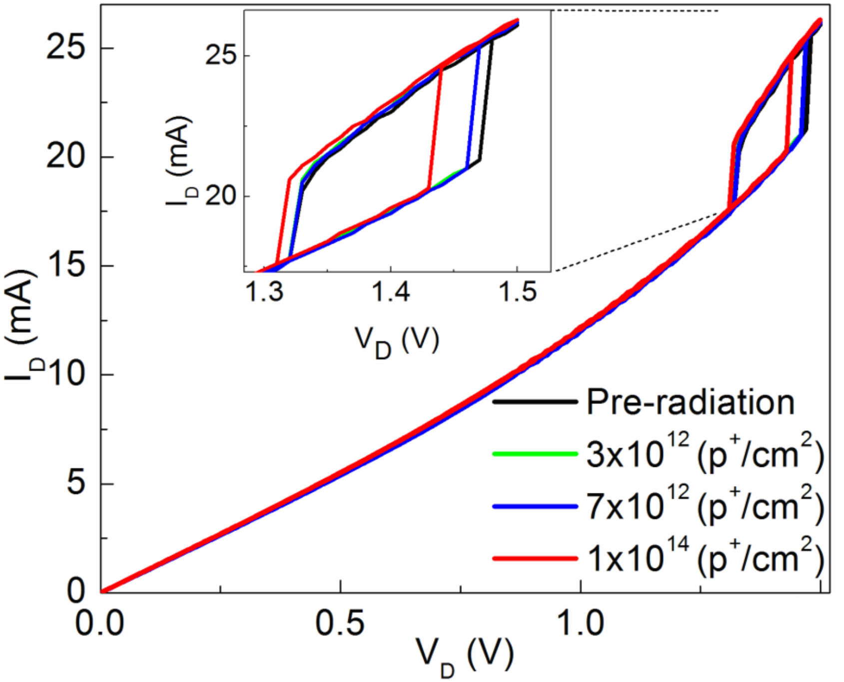

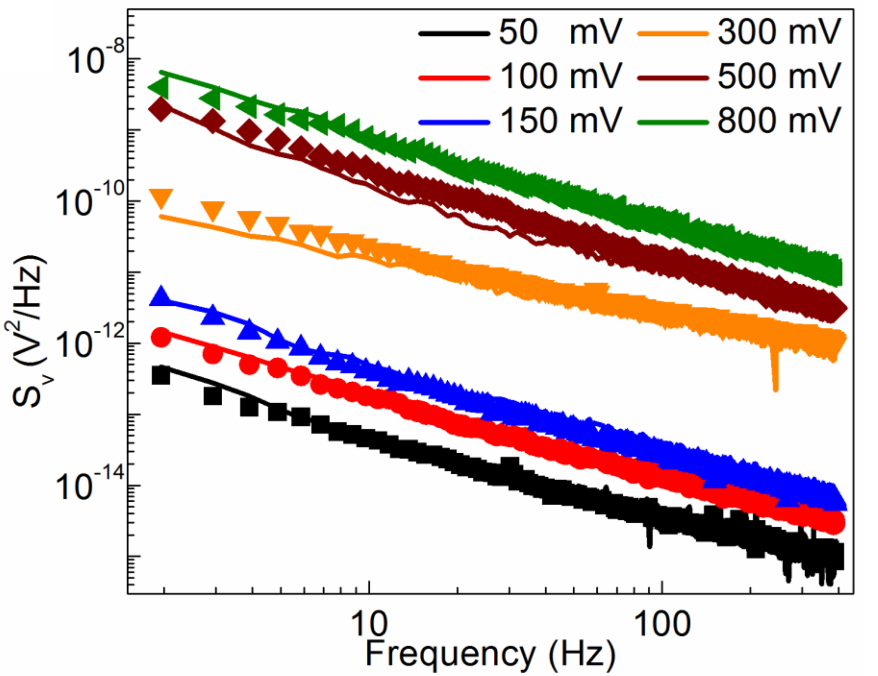

The quasi-two-dimensional (2D) 1T-TaS_2 channels show a *remarkable* immunity to bombardment with the high-energy 1.8 MeV protons to, at least, the irradiation fluence of 10^{14} H^+cm^{-2}.

A. K. Geremew, F. Kargar, E. X. Zhang, S. E. Zhao, E. Aytan, M. A. Bloodgood, T. T. Salguero, S. Rumyantsev, A. Fedoseyev, D. M. Fleetwood and A. A. Balandin, Nanoscale, 11, 8380 (2019).

Noise Spectroscopy of CDW Transitions

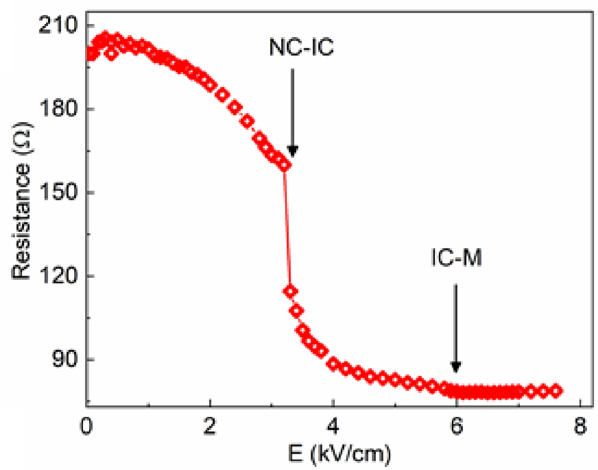

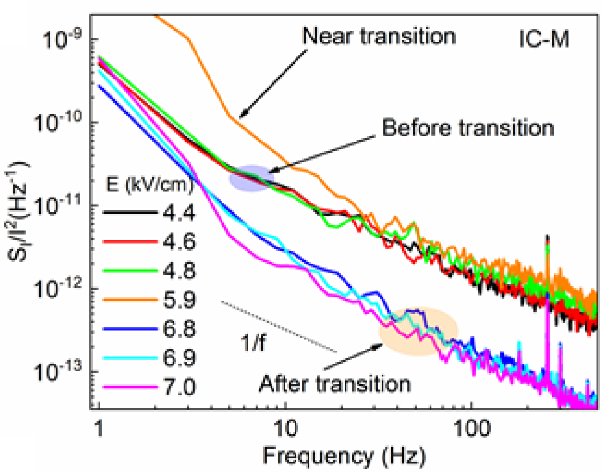

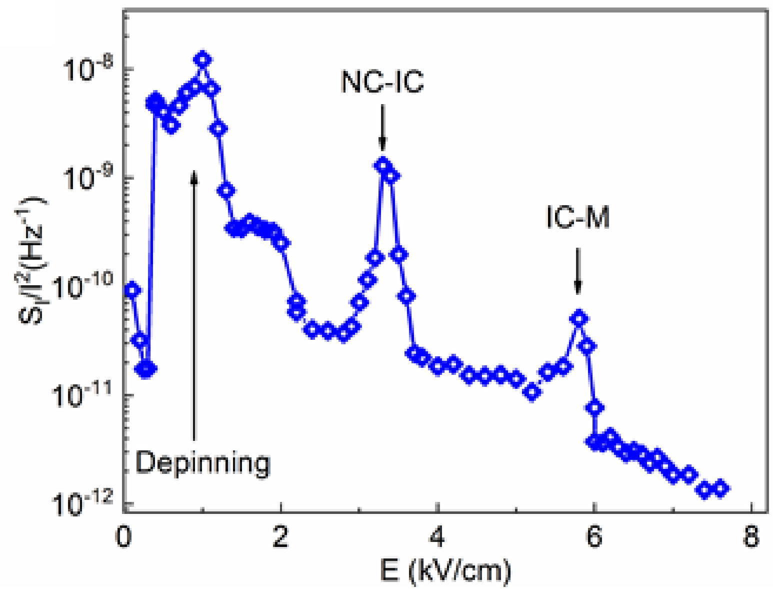

→ Resistance as a function of the applied electric field measured at RT.

→ Noise spectral density as the function of frequency for several values of the electric field, which include the point of transition from the IC-CDW to the normal metallic phase.

→ Noise spectral density, measured at f=10 Hz, as the function of the electric field.

A. K. Geremew, S. Rumyantsev, F. Kargar, B. Debnath, A. Nosek, M. A. Bloodgood, M. Bockrath, T. T. Salguero, R. K. Lake, and A. A. Balandin, ACS Nano, 13, 7231 (2019).

Electric Field *vs* Self-Heating Mechanism in CDW Devices

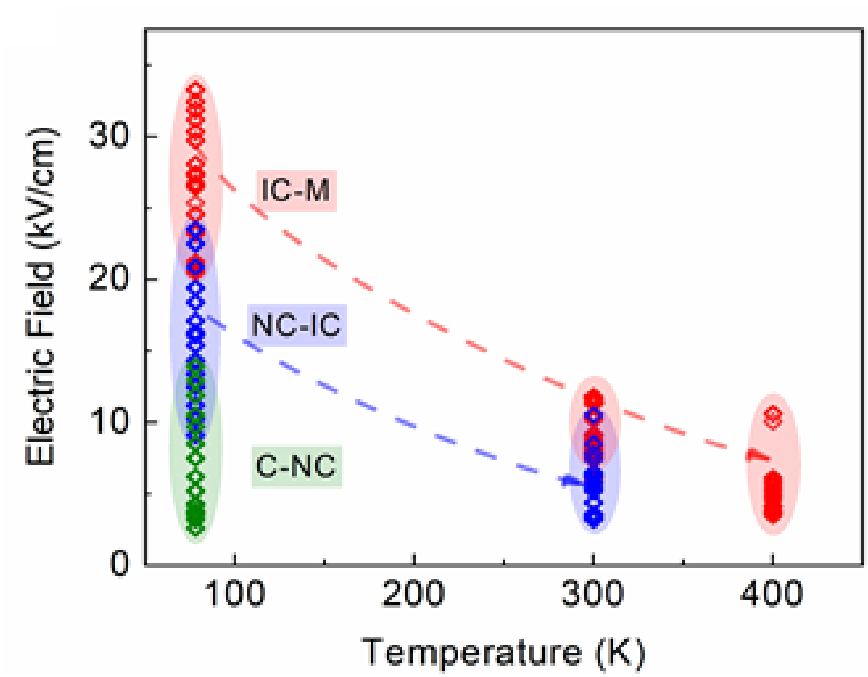

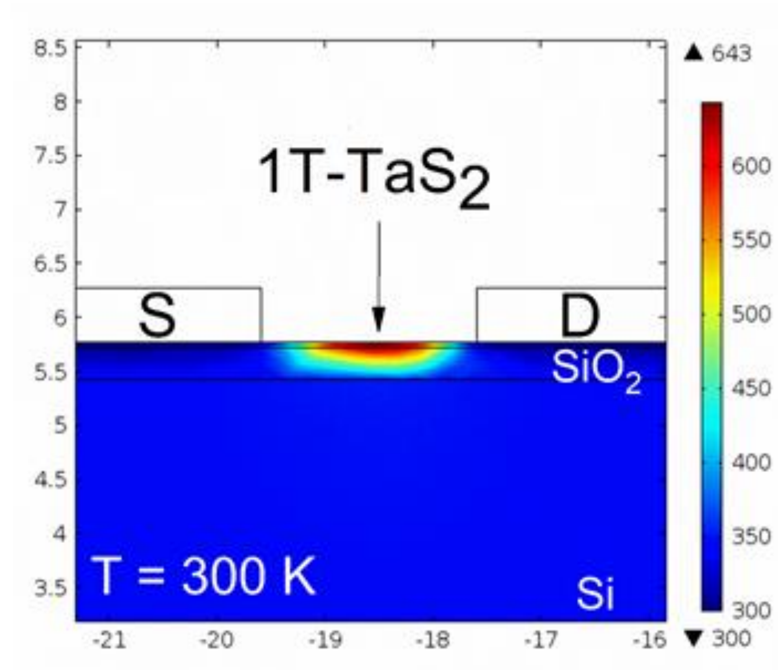

Summary of electric field induced phase transitions at different temperatures for 1T-TaS_2 devices. The variation in the electric field required to include the phase transitions is due to different device geometries, thickness of the layers in the device structures, and other variations in the device designs.

A. K. Geremew, S. Rumyantsev, F. Kargar, B. Debnath, A. Nosek, M. A. Bloodgood, M. Bockrath, T. T. Salguero, R. K. Lake, and A. A. Balandin, ACS Nano, 13, 7231 (2019).

Can the CDW Switching be Fast Even If It is Induced by Heating?

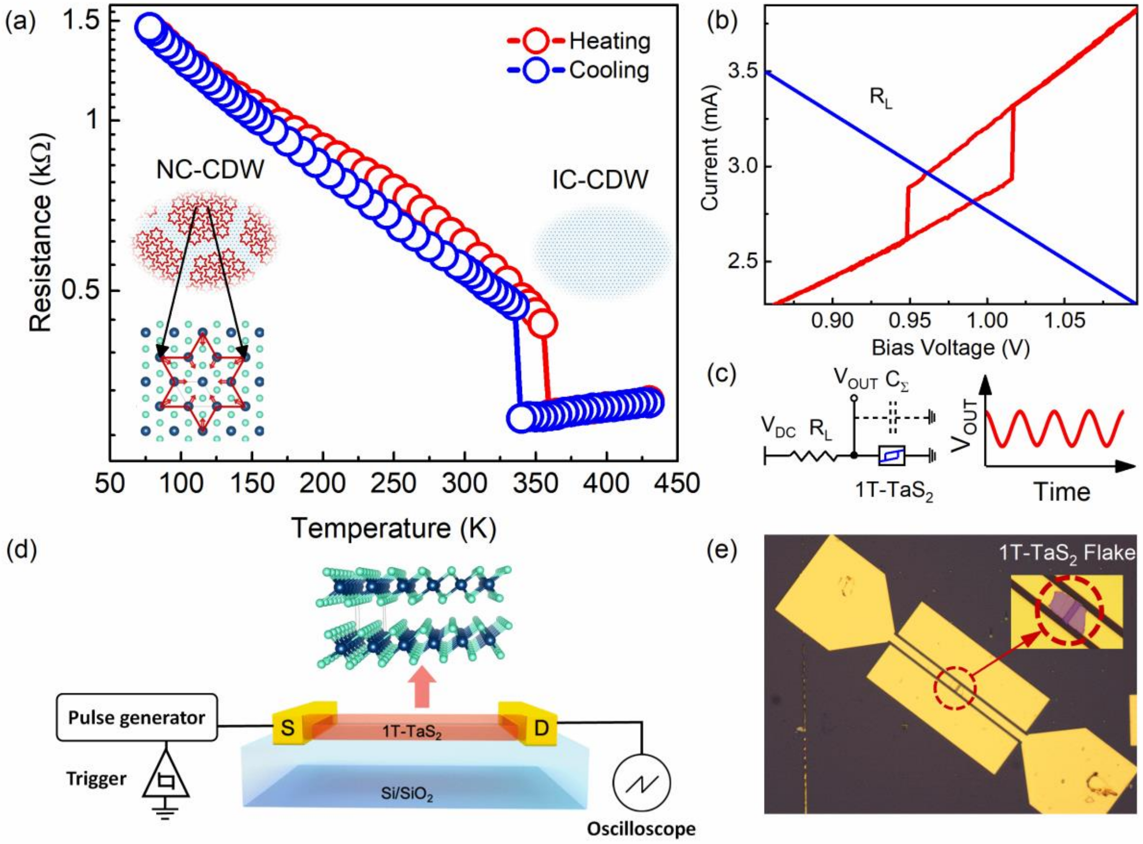

We studied the switching transition between the nearly commensurate and incommensurate CDW phases in $1T\text{-}TaS_2$ films using pulse measurements and numerical simulations.

A pulse generator creates repetitive current pulses as short as 8 ns. The generated current is then measured by a mixed-signal oscilloscope.

A. Mohammadzadeh, *et al*., Appl. Phys. Lett. 118, 093102 (2021).

| Nano-Device Laboratory >

Experimental and Calculated CDW Current-Voltage Characteristics

Experimental

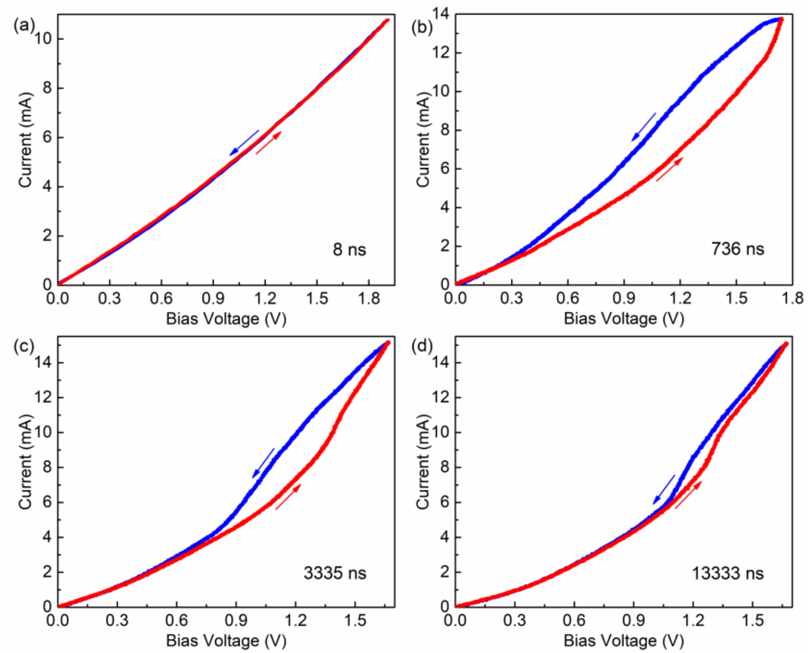

Simulated

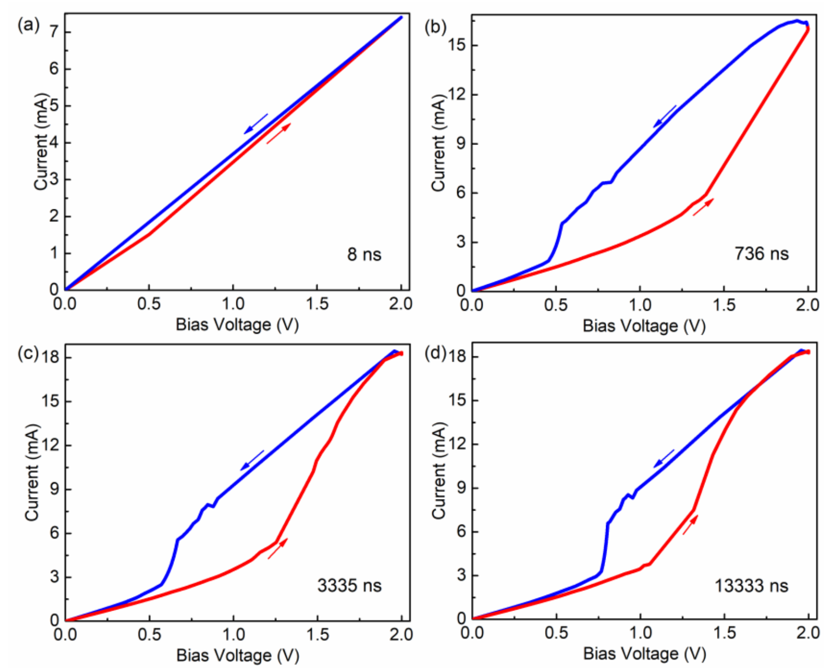

Experimental (left) and simulated (right) I-V characteristics for (a) 8 ns, (b) 736 ns, (c) 3,335 ns, and (d) 13,333 ns pulses. For the shortest duration shown (8 ns), no hysteresis window is observed. With increasing the pulse duration, the width of the hysteresis window expands and then shrinks again. This behavior is attributed to the transient heat diffusion characteristics of the 1T-TaS_2 film, during the up and down sections of the pulse, causing the film to attain different temperatures at fixed bias in the hysteresis region.

A. Mohammadzadeh, *et al*., Appl. Phys. Lett. 118, 093102 (2021).

Thermally Driven CDW Switching

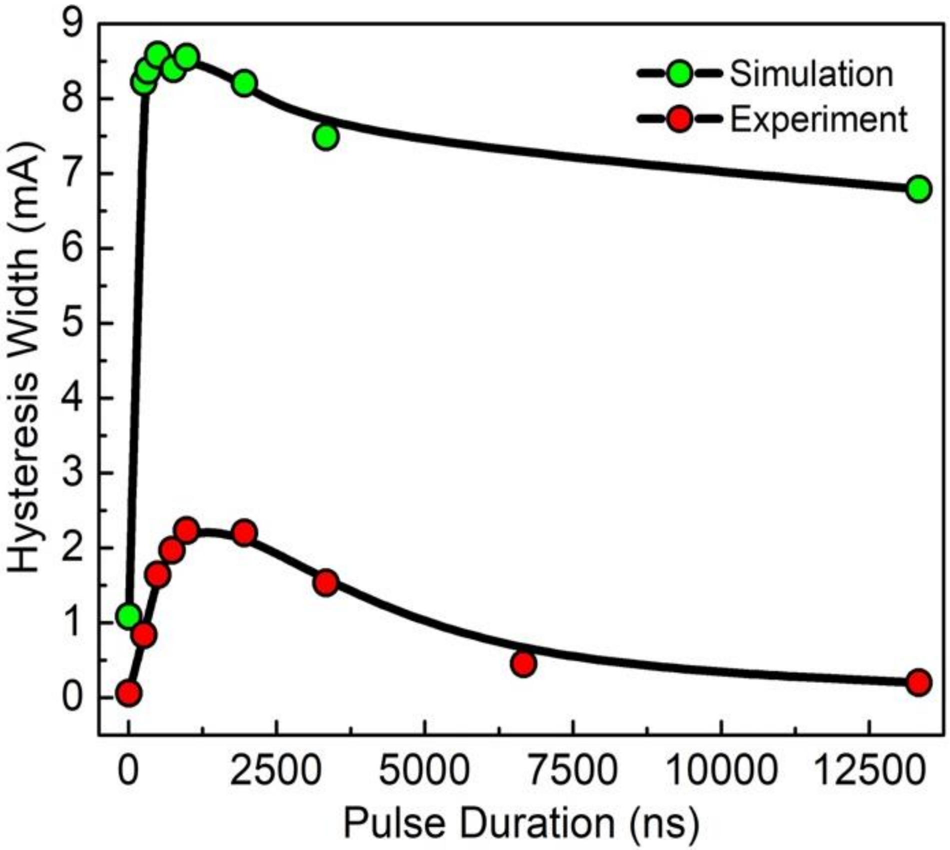

- → Experimental, and simulated hysteresis window width (I_c -I_h) calculated at the constant bias voltage of 1 V as a function of pulse duration. The experimental and theoretical results both follow the same trend, exhibiting a peak at shorter pulse durations and saturating at longer pulse times.
- → Our results do not mean that you cannot achieve electrical switching

A. Mohammadzadeh, S. Baraghani, S. Yin, F. Kargar. J. P. Bird, and A. A. Balandin, “Evidence for a thermally driven charge-density-wave transition in 1T-TaS_2 thin-film devices: Prospects for GHz switching speed” Appl. Phys. Lett., 118, 093102 (2021).

CDW Switching: Prospects of GHz Switching Speed

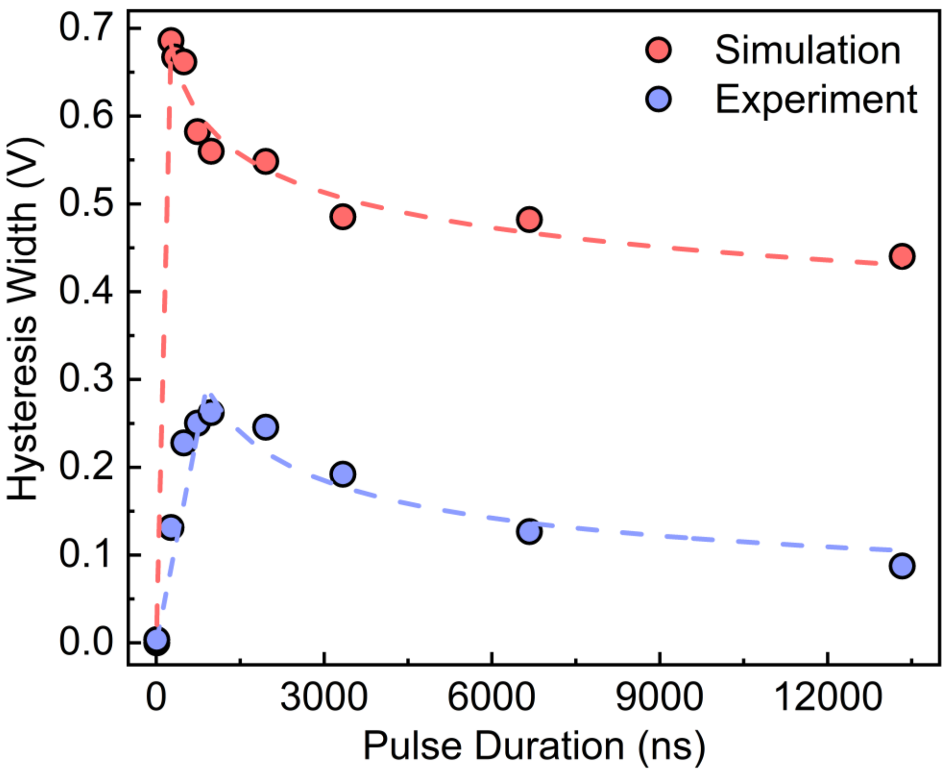

Experimental and simulated hysteresis window width (V_C-V_H) at the constant current of 8 mA and as a function of pulse duration.

We used the experimentally validated model to estimate the device switching speed as the device size decreases. It was found that despite the dominant self-heating effects, tuning of the dimensions can lead to a device that can operate at GHz frequencies.

A. Mohammadzadeh, S. Baraghani, S. Yin, F. Kargar, J. P. Bird, and A.A. Balandin, Thermally-driven charge-density-wave transitions in 1T-TaS_2 thin-film devices: Prospects for GHz switching speed, Appl. Phys. Lett. 118, 093102 (2021) - chosen as the APL Editor's Pick.

The Search for the CDW Depinning and Sliding in Quasi-2D CDW Materials

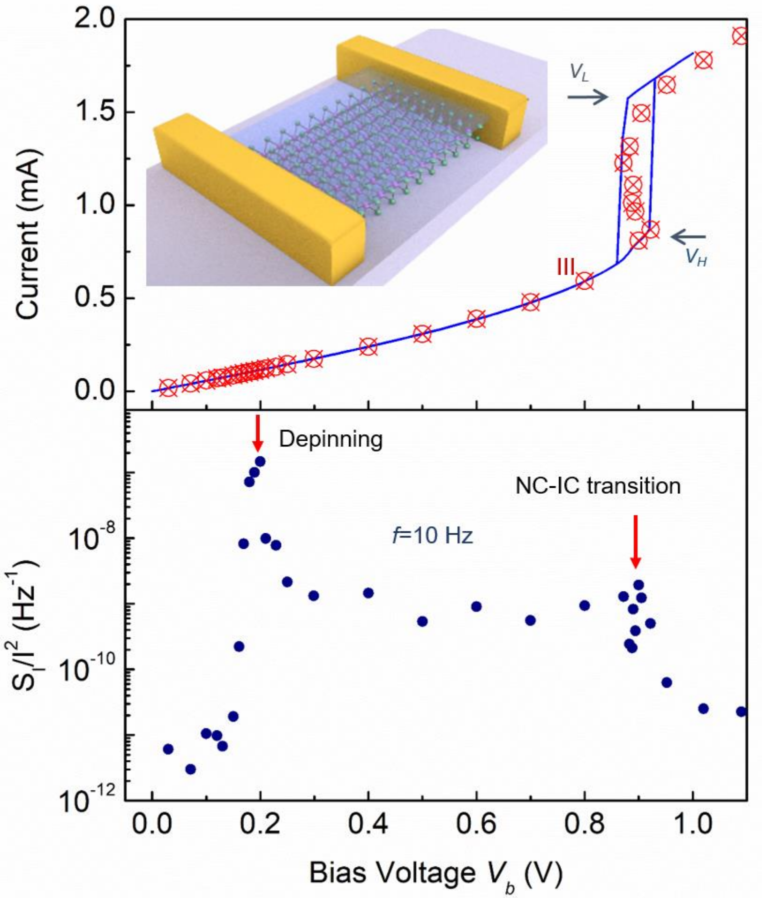

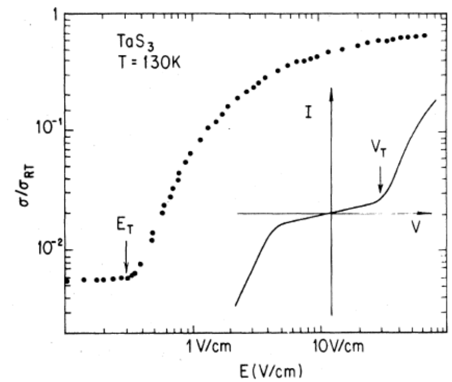

IV-characteristics of 2D CDW materials are different from those of bulk 1D CDW.

G. Gruner, Rev. Mod. Phys., 60, 1129 (1988).

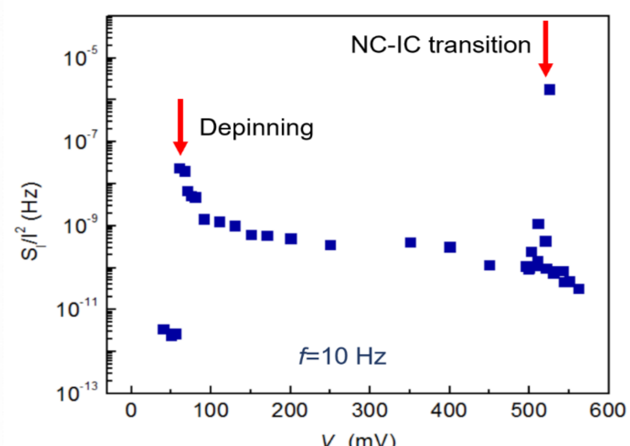

Noise is more sensitive than I-Vs for monitoring CDWs in quasi-2D materials

G. Liu, S. Rumyantsev, M. A. Bloodgood, T. T. Salguero, and A. A. Balandin, Nano Letters, 18, 3630 (2018).

The Signatures of the "Narrow Band Noise" in Quasi-2D CDWs

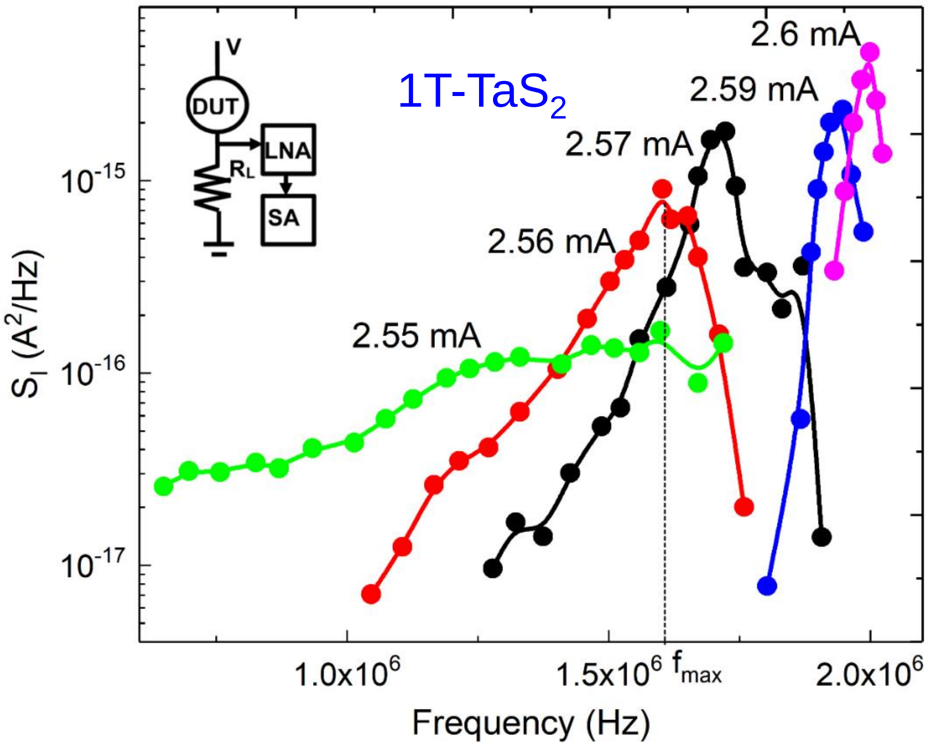

Noise as a function of frequency for several value of the current through the device channel. The peak shifts to the higher frequency f_o with the increasing current.

In bulk quasi-1D CDW materials, the linear relationship was explained assuming that *f* is proportional to the CDW drift velocity, v_D, so that $f=v_D/\Lambda$, where Λ is the characteristic distance.

Since $I_{CDW}=nef\Lambda A$, where *n* is the charge carrier density, *e* is the charge of an electron, and *A* is the cross-sectional area, one obtains: $f=(1/neLA)\times I_{CDW}$

A. K. Geremew, S. Rumyantsev, B. Debnath, R. K. Lake, and A. A. Balandin, "High-frequency current oscillations in charge-density-wave 1T-TaS2 devices: Revisiting the “narrow band noise” concept," Appl. Phys. Lett., 116, p. 163101 (2020).

Have We Found the "Narrow Band Noise" in Quasi-2D CDWs?

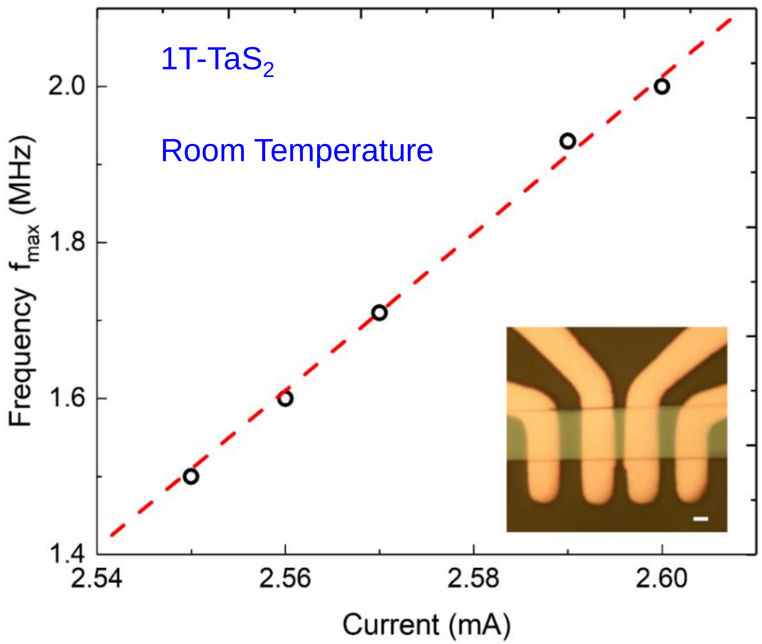

Frequency, f_o of the noise peaks as a function of the current through 1T-TaS_2 device channel. The inset shows a microscopy image of a representative 1T-TaS_2 device structure with several metal contacts.

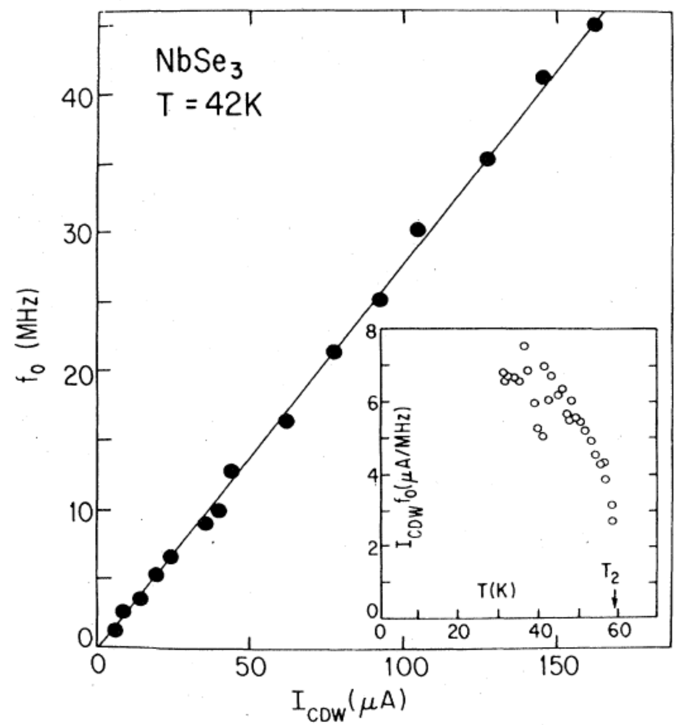

Relation between the COW current and fundamental oscillation frequency in $NbSe_3$. The inset shows I_{CDW}/f_o vs. temperature. After Bardeen et al. (1982).

Alexander A. Balandin, University of California - Riverside

| Nano-Device Laboratory >

The Current Oscillations are due to Hysteresis at the NC-CDW – IC-CDW Transition

The current oscillations appear to be similar to our earlier result – this is not the "narrow band noise."

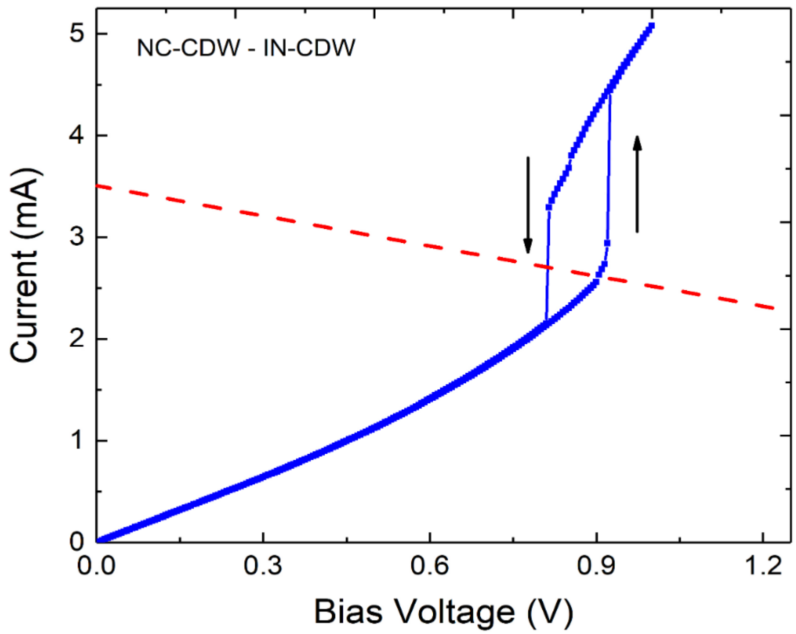

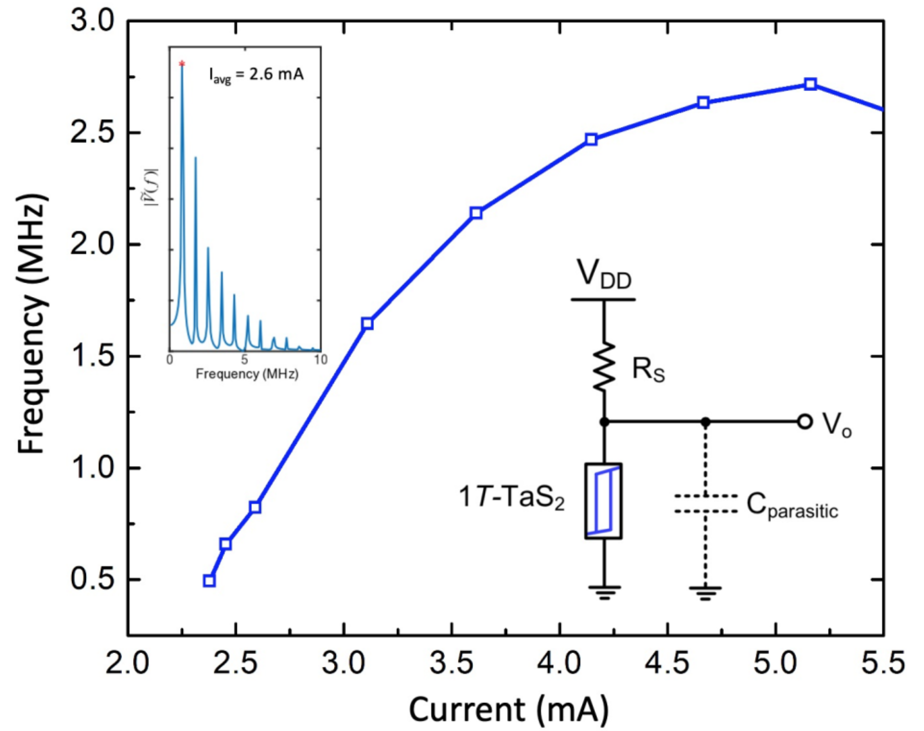

I-Vs of tested 1T-TaS_2 device which revealed "narrow band noise". The hysteresis loop at the bias voltage V = 0.9 V corresponds to the transition from the NC-CDW phase to the IC-CDW phase induced the applied electric field.

Closer Look at I-Vs of 2D CDW Devices

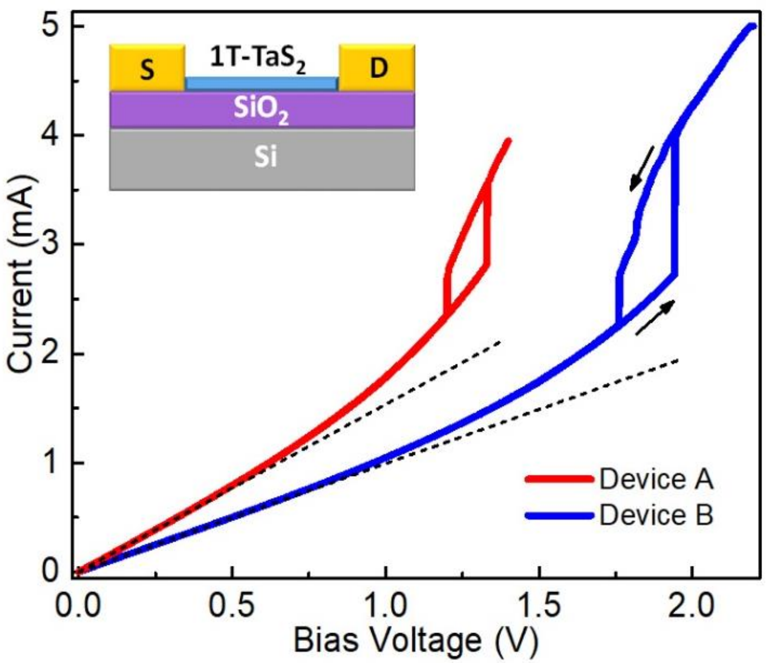

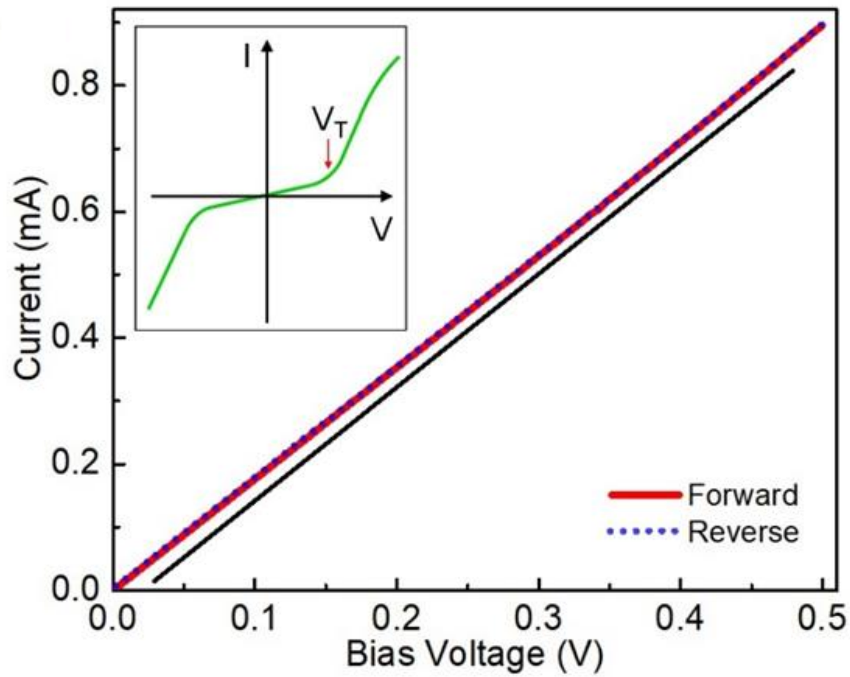

Current-voltage characteristic of the 1T-TaS$_2$ devices on Si/SiO$_2$ substrate at room temperature. The direction of the current sweep is indicated with the arrows. The data are presented for two devices with different channel length fabricated on the same structure. The arrows indicate the direction of the current sweep.

Derivatives of the I-V Characteristics

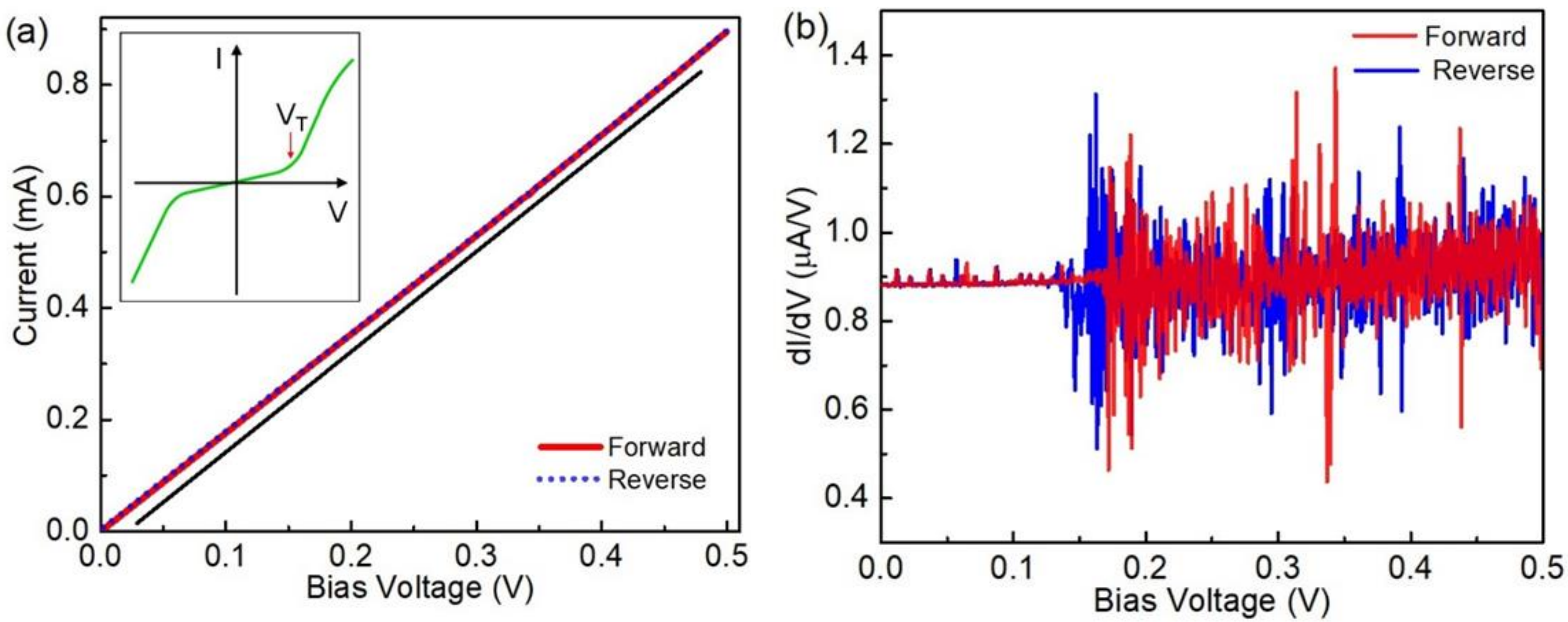

(a) The current in the forward (red) and reverse (blue) sweeping overlaps. The straight black line is shown for comparison. No deviations from the non-linearity are observed in this bias range. (b) The derivative of current-voltage characteristics revealing a strong change in the electron transport.

The threshold in 2D is ~1 kV/cm while in 1D systems it is ~ 40 mV/cm – 4 V/cm

Noise Spectroscopy Reveals the Depinning in 2D 1T-TaS_2 CDW Devices

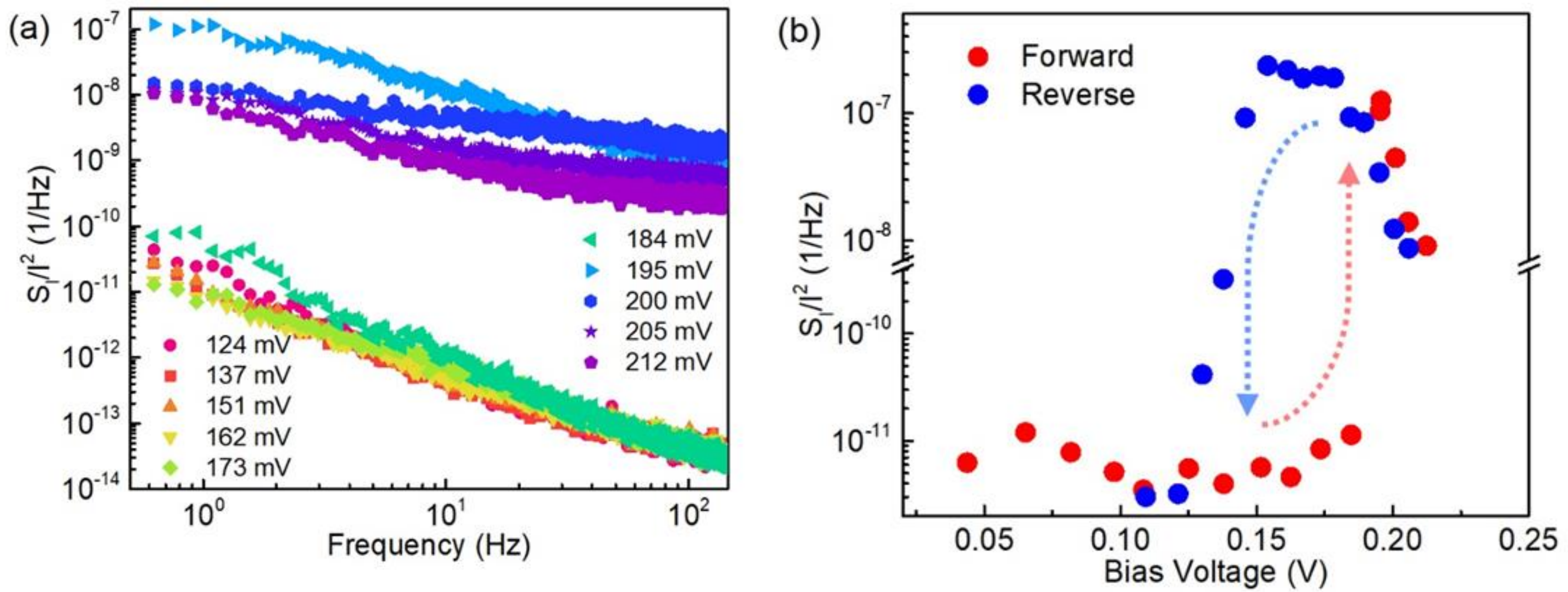

A. Mohammadzadeh, A. Rehman, F. Kargar, S. Rumyantsev, J. M. Smulko, W. Knap, R. K. Lake, and A. A. Balandin, "Room-temperature depinning of the charge-density waves in quasi-2D 1T-TaS2 devices", Appl. Phys. Lett., 118, 223101 (2021).

Likely Signatures of Sliding CDWs in 2D Materials

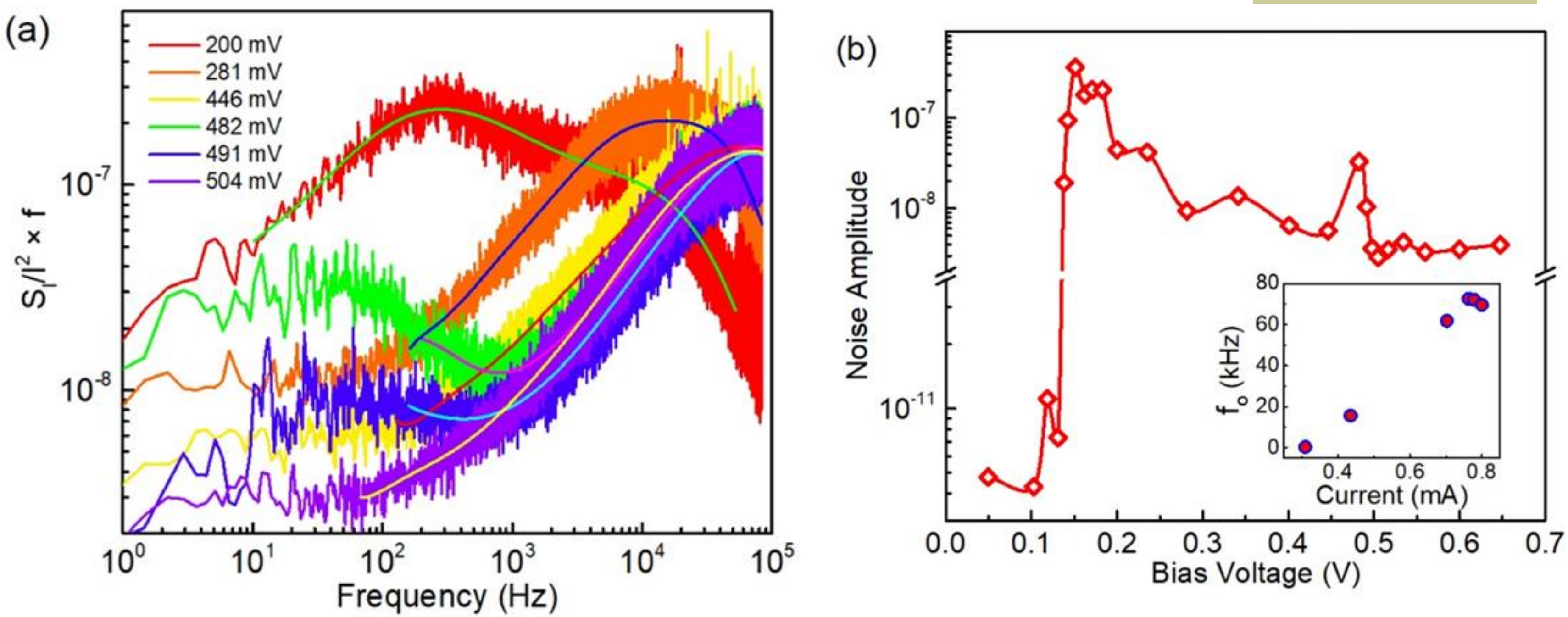

(a) Normalized noise spectral density multiplied by the frequency, $S_I/I^2\times f$, as a function of frequency at different applied bias voltages. (b) The noise amplitude as a function of the bias voltage. Note the break in the y-axis. The noise level experiences a drastic increase at the depinning point. The inset shows the dependence of the corner frequencies with the current in the device channel.

→ Extremely small contribution of CDW current to the total current in 2D systems

Take Home Messages

→Quasi-1D van der Waals materials are as interesting as quasi-2D van der Waals materials

→ Going from quasi-2D to quasi-1D brings a lot of new functionalities and potential applications

→The charge-density-wave quantum materials and devices field is in a rapid growth mode

→ The rebirth of the CDW field is to a large degree due to going from quasi-1D to quasi-2D van der Waals materials

To appear – Special issue of Applied Physics Letters edited by Alexander A. Balandin, Sergei V. Zaitsev-Zotov, and George Grüner (2021)

Acknowledgements

Riverside, California, 2020

| Nano-Device Laboratory >

UCLA Samueli
Materials Science & Engineering

Materials Science and Engineering Seminar Series | Fall 2021

Friday, October 8, 2021 | 10:00 AM – 11:00 AM Pacific Time

Quasi 2D and 1D van der Waals Materials – Properties and Device Applications

Alexander A. Balandin, Ph.D.
Professor
University of California, Riverside